Inorganic Chemistry Communications 179 (2025) 114692

Contents lists available at ScienceDirect

Inorganic Chemistry Communications

journal homepage: www.elsevier.com/locate/inoche

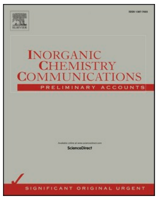

Research Article

Adsorptive removal of uranium(VI) from aqueous solutions using amine-modified chitosan: Kinetics, isotherms, thermodynamics, and its mechanistic insights

Venkata Subbaiah Munagapati [a], Hsin-Yu Wen [b], Anjani R.K. Gollakota [c], Jet-Chau Wen [a,d,*], Kun-Yi Andrew Lin [e,f,**], Yuvaraja Gutha [a,g], Chi-Min Shu [d], Vijaya Yarramuthi [h]

[a] Research Centre for Soil & Water Resources and Natural Disaster Prevention (SWAN), National Yunlin University of Science and Technology, Douliu, Yunlin 64002, Taiwan
[b] Department of Pathology, West China Hospital, Sichuan University, Chengdu 610041, China
[c] Department of Chemical and Materials Engineering, National Yunlin University of Science and Technology, Douliu, Yunlin 64002, Taiwan
[d] Department of Safety, Health, and Environmental Engineering, National Yunlin University of Science and Technology, Douliu, Yunlin 64002, Taiwan
[e] Department of Environmental Engineering & Innovation and Development Center of Sustainable Agriculture, National Chung Hsing University, Taichung, Taiwan
[f] Institute of Analytical and Environmental Sciences, National Tsing Hua University, Hsinchu, Taiwan
[g] Guangdong Provincial Key Laboratory for Radionuclides Pollution Control and Resources, School of Environmental Science and Engineering, Guangzhou University, Guangzhou 510006, China
[h] Department of Chemistry, Vikrama Simhapuri University, Nellore 524320 Andhra Pradesh, India

ARTICLE INFO

Keywords:
Amine-modified chitosan
Uranium(VI)
Removal
Regeneration

ABSTRACT

The discharge of uranium into aquatic systems from industrial nuclear waste poses a significant risk to the environment and ecological balance. Consequently, it is necessary to create affordable and eco-friendly biosorbents with high adsorption capacity to remove U(VI) pollutants from the liquid phase. In the present research work, a novel amine-modified chitosan (AMCS) adsorbent was synthesized through a multi-step chemical modification process involving chlorination, Schiff base formation, and subsequent amine functionalization, which was utilized for the removal of U(VI) from aqueous environments. This simple and cost-effective cross-linking approach introduces various functional groups into the chitosan, increasing its attraction to U(VI) ions. The synthesized AMCS were systematically characterized through SEM (with elemental mapping), BET, FTIR, ^{1}H NMR, and ^{13}C NMR spectral analysis. Batch adsorption tests were performed to assess the impact of pH, U(VI) ion concentration, AMCS dose, contact duration, and temperature. A maximal removal efficiency of 94.5 % was achieved under optimal conditions: pH 5.0, AMCS dose 0.7 g, contact duration 140 min, initial concentration 50 mg/L, and temperature 298 K. The maximum monolayer adsorption uptake of U(VI) on AMCS was found to be 287.7 mg/g at 298 K. The value of pH for the AMCS was obtained at about 5.3. The equilibrium sorption data aligned well with the Langmuir model, while the kinetic data were best described by the pseudo-second-order model. The sorption process was influenced by film and intraparticle diffusion mechanisms. The thermodynamic variables entropy ($\Delta S^\circ = 100$ J/mol K), enthalpy ($\Delta H^\circ = 4.698$ kJ/mol) and Gibbs free energy (-25.146, -26.131, -27.149 at 298, 308 and 318 K, respectively), indicated that the sorption of U(VI) onto AMCS was spontaneous, endothermic and feasible. After regenerations, the morphology of AMCS was still maintained, and the U(VI) adsorption efficiency remained above 75 %, manifesting the excellent cycle performance of AMCS.

---

* Corresponding author at: Research Centre for Soil & Water Resources and Natural Disaster Prevention (SWAN), National Yunlin University of Science and Technology, Douliu, Yunlin 64002, Taiwan.

** Corresponding author at: Department of Environmental Engineering & Innovation and Development Center of Sustainable Agriculture, National Chung Hsing University, Taichung, Taiwan.

E-mail addresses: wenjc@yuntech.edu.tw (J.-C. Wen), linky@nchu.edu.tw (K.-Y.A. Lin).

https://doi.org/10.1016/j.inoche.2025.114692
Received 8 January 2025; Received in revised form 12 May 2025; Accepted 15 May 2025

1. Introduction

Water is a fundamental need for all living organisms in the world. The primary water source for human consumption was obtained from the rivers. Most of the world's civilizations have evolved on riversides historically. The majority of the industries and plants are located in the vicinity of water bodies. However, the discharge of pollutants into these aquatic systems has severely damaged the ecological balance and poses significant risks to human health through processes such as biomagnification [1]. When water becomes contaminated with various pollutants, it can lead to numerous illnesses and adverse health effects upon consumption. With the rapid development of the atomic sector, fatal and radioactive levels of uranium were disposed of into the atmosphere from uranium mining, nuclear energy plants and refining operations [2–8]. Uranium can exist in two oxidation states, i.e., U(IV) and U(VI). Significant health effects due to U(VI) poisoning are damage to brain, liver and kidney functions and various cancers and genetic mutations if directly connected with skin [9]. As a result, practical and cost-effective techniques were explored to eliminate U(VI) from aqueous, seawater, atomic wastewater, and sewage industries.

A variety of processes, including chemical precipitation [10], catalytic ozonation [11], ion exchange [12], photodegradation [13], electrodeposition [14], solid-phase extraction [15,16], capacitive deionization [17], and adsorption [18–21], were applied for the elimination of uranium and other metal ions from different polluted sources. Due to efficiency, operational comfort and excellent feasibility, the adsorption technique has become quite important. Regarding costs and technical requirements, every material has diverse effects on the removal process. However, most of the adsorbents are non-biodegradable, creating supplementary pollution. Recently, many adsorbents have been made using biodegradable materials such as chitosan and alginate to solve this issue. Chitosan, a polymer of N-acetyl-d-glucosamine & β(1-4)-linked d glucosamine units, is obtained through the deacetylation of chitin. After cellulose, chitosan is one of the largest and most abundant natural polyaminosaccharide. Chitosan with chemical modification fascinated abundant attention due to its strong adsorption capability for adsorbing distinct pollutants. Chemically modified chitosan adsorbent can potentially adsorb different pollutants from various solutions [22,23]. Chitosan received significant attention in the sorption process because of its low cost, easy accessibility, low toxicity, chemical reactivity, biodegradability, non-toxic and hydrophilic nature [24].

Chemical changes in chitosan are the primary concern as they would not alter the basic chitosan skeleton, maintain the initial physicochemical and biochemical characteristics, and eventually produce enhanced characteristics [25]. Applying chitosan or modified chitosan sorbents removes U(VI) ions from wastewater by potential techniques. Carbonaceous Nanofibers [26], MnO_2@PPy [27], Amidoxime modified chitosan/bentonite composite [28], Magnetic amidoxime-functionalized chitosan beads [29], Amidoxime-functionalized magnetic chitosan micro-particles [30], α-aminophosphonate functionalized chitosan [31], Polyvinylpyrrolidone/Chitosan blended nanofibers [32], CuO/X zeolite based nanocomposites [33], graphene oxide–carbon nanotubes hybrid aerogels [34], polysulfide/layered double hydroxide composites [35], zero-valent iron loaded chitosan [36], agmatine ligand functionalized magnetic alginate beads [37], MP/SiO_2/p(GMA)-AO [38], amine/carboxyl groups modified cellulose beads [39], MGO@Si-DADAO particles [40] and TAEA and PEIM ligang decorated p(GA-EGMA) microbeads [41] was extensively applied for U(VI) removal. Even though more and more adsorbents are still required to eliminate U(VI) from an aqueous and polluted environment, To overcome the problem here, we prepared a simple and novel with high sorption capacity sorbent material and utilized it for U(VI) removal. According to the authors, there are no scientific reports on the synthesis and assessment of AMCS as a biosorbent for eliminating U(VI) ions from aquatic environments.

The novelty of this study lies in developing and characterizing a new adsorbent material, AMCS, which proves to be highly efficient in eliminating U(VI) from contaminated wastewater. To date, no researcher has explored using this adsorbent for U(VI) removal. Consequently, this study introduces an innovative and effective solution for treating U(VI) in contaminated water. It showcases the adsorbent's exceptional performance and reusability, emphasizing its potential for removing radioactive metals. This research presents a unique approach to water purification by launching an adsorbent that boasts unparalleled efficiency, reusability, and adaptability in addressing U(VI) pollutants.

In the present work, AMCS was synthesized using a simple and inexpensive crosslinking technique and applied to eliminate U(VI) ions from aquatic environments. Various parameters influencing the uptake of U(VI) from aquatic environments, such as contact duration, pH solution, AMCS dose, temperature, and U(VI) concentration, on the sorption process were assessed. Subsequently, SEM (with elemental mapping), BET, FTIR, ^{1}H NMR, and ^{13}C NMR spectral analysis were employed to characterize the AMCS. Adsorption isotherms, kinetics and thermodynamics were studied to assess the sorption performance of U(VI). Additionally, tests of the reusability of the adsorbent were conducted to gauge its potential for sustainable and commercial applications.

2. Materials and methods

2.1. Materials

Chitosan (degree of deacetylation: >85 %, molecular mass: 110,000 g/mol, viscosity: 100–200 mPa.s), 3-chloropropanoyl chloride, thiosemicarbazide, benzaldehyde, thionyl chloride and semicarbazide were used and purchased from Sigma-Aldrich. $UO_2(NO_3)_2{\cdot}6H_2O$ (Uranyl nitrate hexahydrate) was procured from Hubei Chushengwei Chemical Co., Ltd., China. All substances utilized in this research were acquired and were commercially accessible.

2.2. Adsorbate preparation

An appropriate quantity of $UO_2(NO_3)_2{\cdot}6H_2O$ was dissolved in deionized water (DI) to formulate a U(VI) stock solution with a concentration of 300 mg/L. The desired standard solutions were obtained by diluting the stock solutions with an appropriate volume of DI water.

2.3. Adsorbent preparation

The AMCS was prepared following the cross-linking method. Initially, 2 g of chitosan was melted by agitation in 100 mL of a 2 % (v/v) acetic acid solution, and this reaction blend was stirred for 3–4 h until a homogeneous solution was obtained without any air bubbles. Later, 3-chloropropanoyl chloride was added to this homogeneous solution, which had already been dissolved in 30 mL of methanol and kept at room temperature with persistent stirring for 4 h. Resulted in the formation of chloropropanoyl-linked chitosan product (CLCP). A very trace amount of CLCP was used for spectral analysis. Add thiosemicarbazide to the solution containing the CLCP reaction mixture and shake for 1 h, producing thiosemicarbazide reacting with CLCP and forming the TC-CLCP product. Further, benzaldehyde was added to TC-CLCP, followed by 20–30 mL of methanol and stirred for 2 h. Schiff's base formation can occur through the free amino groups with the benzaldehyde, and we got the Sc-TC-CLCP. After that, thionyl chloride was added drop by drop to Sc-TC-CLCP, and the reaction proceeded at 60 °C for 3 h. As a result, the –OH group at C_3 was swapped by the chlorine group. Consequently, chlorinated Sc-TC-CLCP was obtained. Finally, 25 mL of methanol and semicarbazide were added to chlorinated Sc-TC-CLCP (Cl- Sc-TC-CLCP), and the reaction was continued at 60 °C for 3 h. Ultimately, we got the amine-modified chitosan derivative and named it AMCS for further representation. The total synthesis part and final product image are shown in Scheme 1.

2.4. Adsorption experiments

All the tests were carried out in batch mode sorption process with various operating variables like contact duration, pH, temperature, AMCS dose, and U(VI) ion concentration. The pH tests were conducted using 30 mL of U(VI) ion solution (50 mg/L) and 0.5 g of AMCS in 50 mL conical flasks. pH solution was adjusted with 0.1 M-NaOH/HCl, and the tests varied between 1.0 and 10.0. Adsorbent dosage experiments of AMCS onto U(VI) ions were conducted by changing the amount of biosorbent between 0.1 and 0.7 g. Contact duration was varied from 0 to 180 min. The kinetic test was conducted in a 50 mL conical flask containing 0.5 g of AMCS and 30 mL U(VI) solution with a 50 mg/L starting concentration. Equilibrium studies of AMCS onto U(VI) ions were carried out at different temperatures. Once the equilibrium was established, the biosorbent sample was separated from the solution using filter paper, and ICP-AES was used to determine the concentration of U(VI). All U(VI) sorption studies were executed in duplicate, and the average of the two values was used for the calculation. The following equation achieved the adsorbed quantity of U(VI) at equilibrium:

$$q_e = \frac{(C_i - C_e)V}{M} \tag{1}$$

where C_i and C_e (mg/L) were the starting and final levels of U(VI), V (L) was the volume of U(VI) solution, q_e (mg/g) was the sorption uptake at

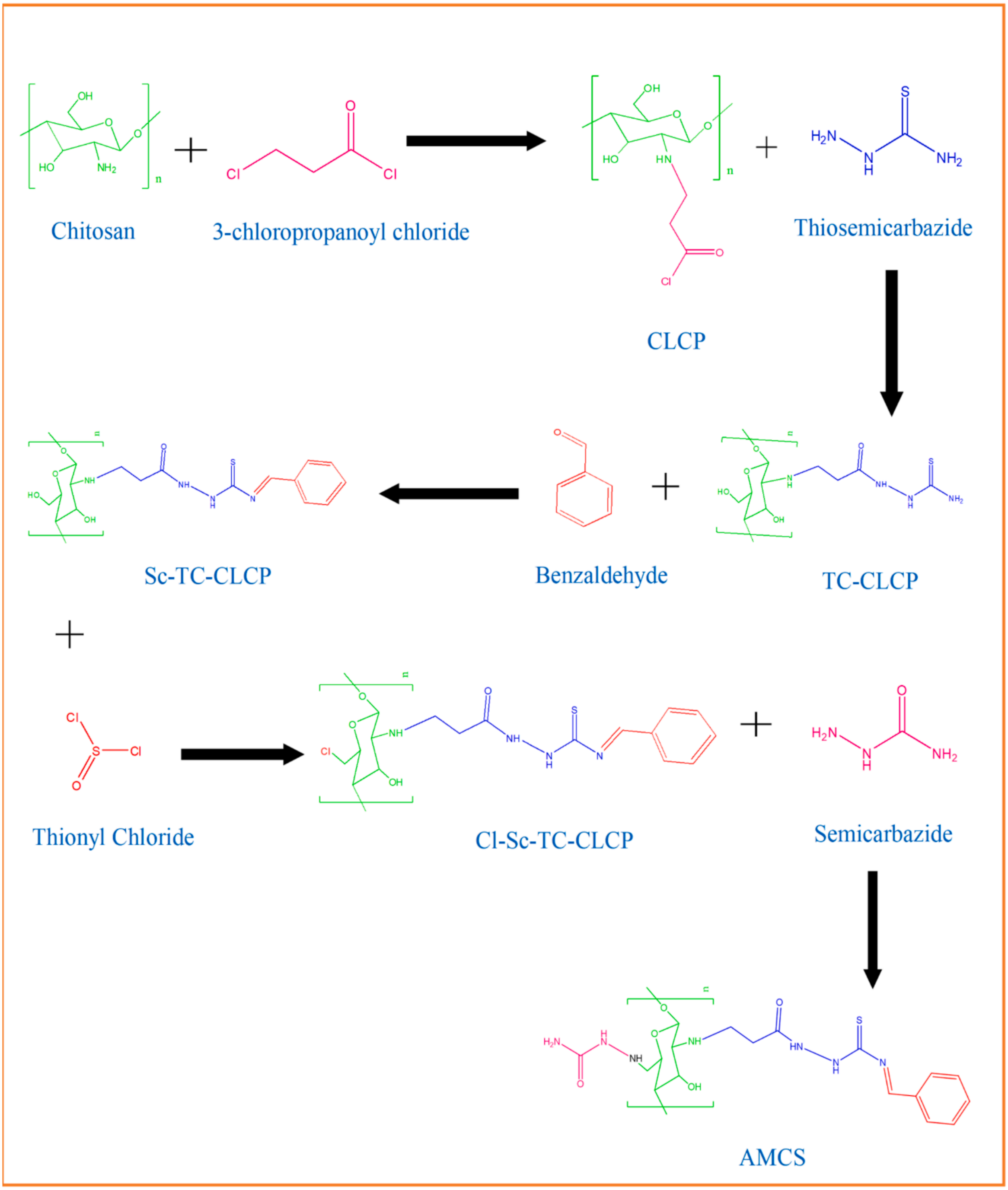

Scheme 1.

equilibrium, and M (g) was the quantity of AMCS.

2.5. *Desorption and reusability of AMCS*

U(VI) desorption from AMCS was investigated using varying concentrations (0.1–0.4 M) of NaOH as the eluent. Initially, 0.5 g of fresh AMCS was mixed with 30 mL of a 50 mg/L U(VI) solution at a pH of 5.0 for 140 min. The residual U(VI) concentration was assessed using ICP-AES to determine how much U(VI) was adsorbed. Next, the unadsorbed U(VI) was removed by sensing the U(VI)-loaded AMCS with DI water. Ultimately, desorption from AMCS was performed by mixing it for a specified duration with 30 mL of each desorption eluent concentration, and the resulting filtrate was analyzed to quantify the U(VI) desorbed from AMCS. During the desorption process, the AMCS was reused for four additional cycles. The percentage recovery of U(VI), representing the effectiveness of the U(VI) desorption from the AMCS, was calculated using Eq. (2):

$$Desorptionefficiency = \frac{AmountofU(VI)desorbed}{AmountofU(VI)adsorbed}X100 \quad (2)$$

2.6. *Error analysis*

The chi-square (χ^2) and the sum of the square error (SSE) tests were also conducted to determine the best-fit kinetic and isotherm models, as represented by the following Eqs.:

$$\chi^2 = \sum \frac{\left(q_{e,exp} - q_{e,cal}\right)^2}{q_{e,exp}} \quad (3)$$

$$SSE = \frac{\sqrt{\sum (q_{e,cal} - q_{e,exp})^2}}{N} \quad (4)$$

where $q_{e,\mathrm{exp}}$ and $q_{e,cal}$ refer to the experimental and theoretical uptakes (mg/g), respectively, while N denotes the count of experimental observations.

3. Results and discussion

3.1. *AMCS characterization*

3.1.1. *BET analysis*

The AMCS was analyzed using the BJH adsorption/desorption method to determine its pore diameter, pore volume, and surface area. The pore volume, pore size and surface area of AMCS were 0.1778 cc/g, 0.18276 nm, and 58.95 m^2/g. In general, if an adsorbent has the length, size and diameter of the pore, it can have the highest sorption power. Thus, AMCS can be regarded as a popular U(VI) removal sorbent.

3.1.2. *FTIR analysis*

Various reactive functional groups, including hydroxyl, sulphur, carboxyl, carbonyl, amine and amide, were designated feasible sorption sites to bind the metallic ions with the adsorbents. An essential analytical tool is FTIR spectroscopy, which determines the properties of the functional groups existing on any material. Fig. 1A and B demonstrate the FT-IR spectra of AMCS and U(VI)-AMCS. FTIR spectra of AMCS exhibit peaks from 3200 to 3500 cm^{-1}, reflecting the overlap of N–H and O–H stretching vibrations [42]. A band at 3150 cm^{-1} could be attributed to vibrations of NH stretching [42]. The band observed at 1630 cm^{-1} corresponds to C=O groups from the aldehyde and ketones [43]. The peak located at 1560 cm^{-1} represents the primary and secondary amide groups [22]. The 1130 cm^{-1} band is assigned to the C–O vibrations [44].

In the FTIR spectra after U(VI) adsorption, changes in intensity and changes in the location of bands can be observed. The initial change was the increase in the regions from 3500–3200 cm^{-1} to 4200 cm^{-1}, which suggested the participation of the free hydroxyl group in the sorption process. The band was shifted from 3150 to 2946 cm^{-1}, revealing that NH groups were involved in U(VI) sorption. The shift from 1630 to 1647 cm^{-1} reveals the participation of C=O groups in U(VI) biosorption. The significant shift from 1130 to 1147 cm^{-1} also indicates that the C-O groups are mainly involved in U(VI) binding. FTIR analysis shows that a potential mechanism of U(VI) adsorption onto AMCS may be caused by physisorption, ion exchange, and surface complex/precipitation in functional groups.

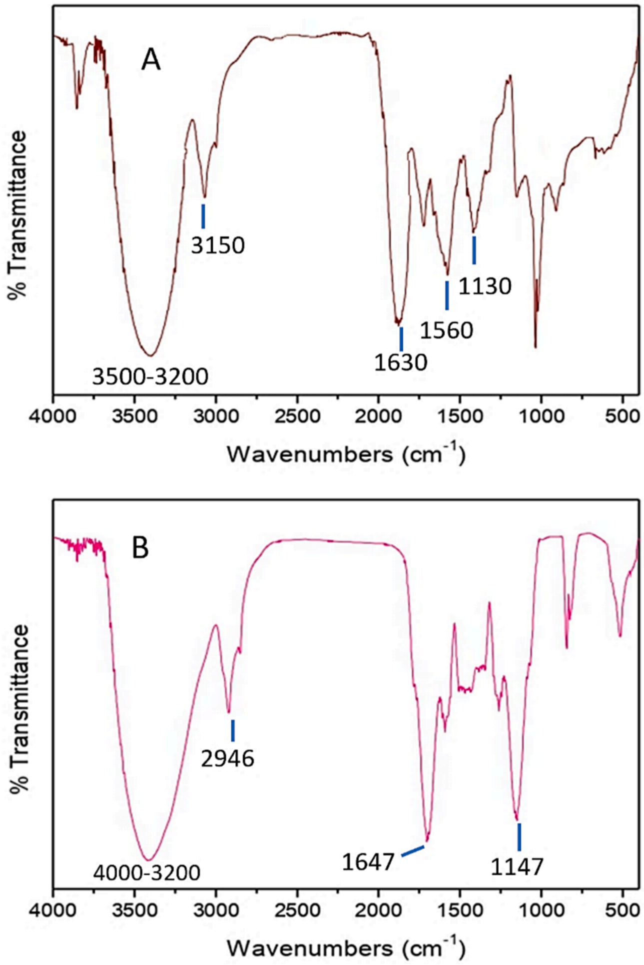

Fig. 1. FTIR analysis of (A) AMCS and (B) U(VI) loaded AMCS.

3.1.3. *SEM micrographs*

SEM with elemental mapping was applied to characterize the biosorbent and elucidate the probable mechanism of adsorption. SEM images of pure AMCS and U(VI) loaded AMCS at different magnifications are shown in Fig. 2A-–D–. AMCS is almost spherical with a smooth surface. The adsorption capacity of AMCS was increased due to its amorphous nature. Significant changes in the surface morphology of the AMCS, as well as the formation of distinct changes, were observed on their surfaces after U(VI) was loaded. We can see clearly from the SEM images of Fig. 2C and D that U(VI) was deposited on the AMCS surface. Pure AMCS (Fig. 2E) exhibited O, N, C, and S elements. After sorption of U(VI), U was found along with O, N, S, and C elements, indicating successful U(VI) biosorption with AMCS.

3.1.4. *^{1}H NMR analysis*

To reach the final chitosan-modified target, initially, begin with preparing propanoyl chloride-linked chitosan (CLCP) from the treatment of 3-chloropropanoyl chloride with chitosan. ^{1}H NMR of CS, CLCP,

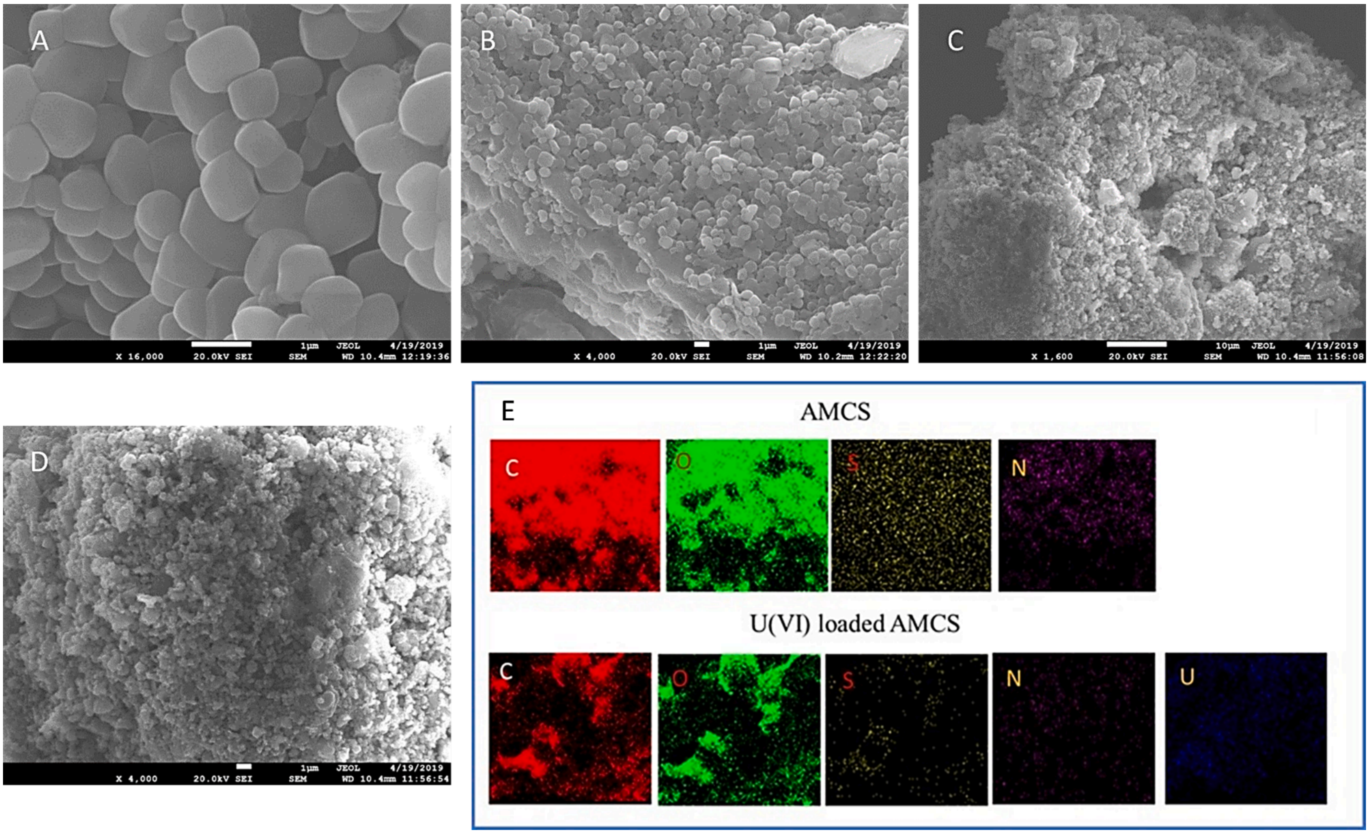

Fig. 2. SEM analysis of (A, B) AMCS; (C, D) U(VI) loaded AMCS; and (E) elemental mapping images of AMCS and U(VI) loaded AMCS.

TC-CLCP, Sc-TC-CLCP, Cl-Sc-TC-CLCP and AMCS was shown in Fig. 3A–F–. The hydrogen spectral data certified the product formation (Fig. 3B, 1H NMR of CLCP). The peak at δ 3.82 ppm fits the two protons of NH linked methylene group; the other carbonyl-linked methylene proton (2H) signal seemed at δ 3.22 ppm, and the remaining spectral values such as δ 3.27, 3.39, 3.65, 3.77, 3.91 and 4.58 ppm were related to chitosan proton peaks. In that data, the peak number 4.58 ppm goes to the second position proton of chitosan. The carbonyl carbon band showed at δ 172.7 ppm, along with starting moiety peaks (chitosan), confirmed the product. Also, the signals at δ 42.6 and 50.8 ppm were related to NH-attached methylene carbon and carbonyl carbon associated with CH_2 carbon.

Later, the above intermediate compound reacted with thiosemicarbazide, followed by the treatment with benzaldehyde, resulting

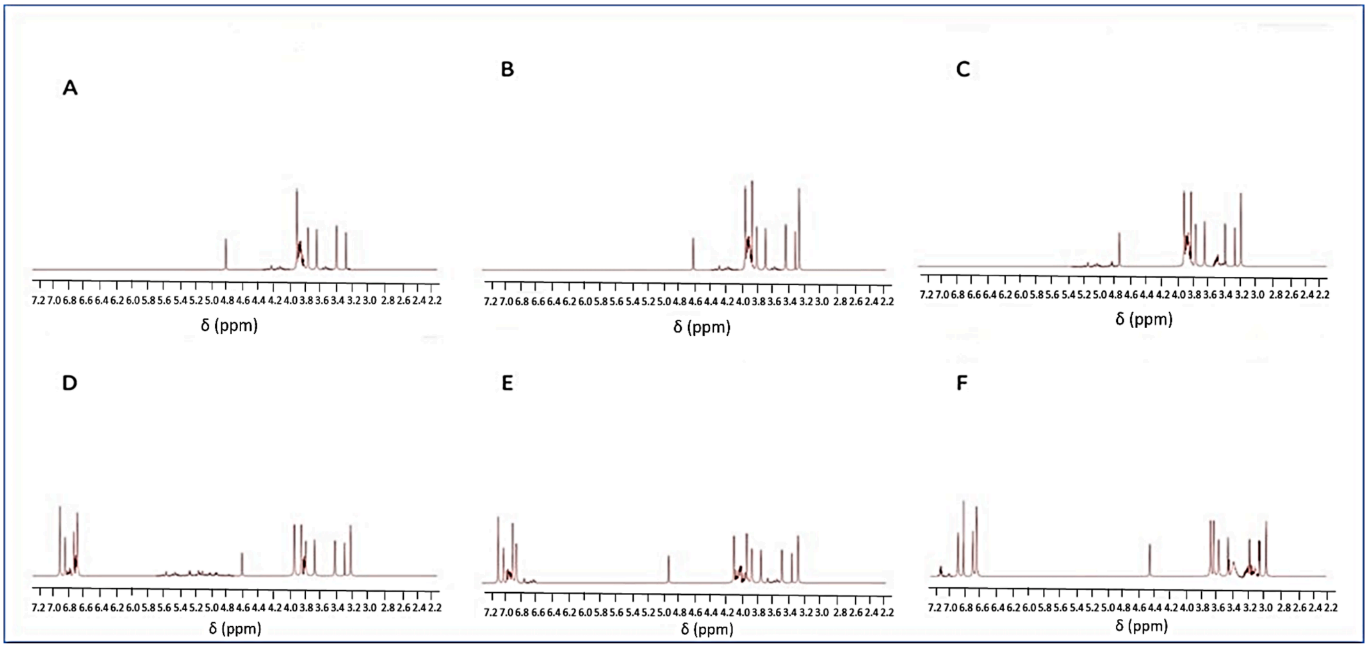

Fig. 3. ^{1}H NMR spectra of (A) CS; (B) CLCP; (C) TC-CLCP; (D) Sc-TC-CLCP; (E) Cl-Sc-TC-CLCP; and (F) AMCS.

in composite Sc-TC-CLCP (^{1}H NMR of TC-CLCP and Sc-TC-CLCP). Then, chlorination of this product (Sc-TC-CLCP) was done with the help of thionyl chloride occurred compound Cl-Sc-TC-CLCP (^{1}H NMR of Cl-Sc-TC-CLCP). The final compound (CAM) was formed by the reaction of Cl-Sc-TC-CLCP with semicarbazide, which was confirmed by hydrogen and carbon spectral data. Peaks found in an aromatic region with the values of δ 6.67 (2H), 6.74 (1H), and 6.87 (2H) ppm belong to benzene ring protons of the product (^{1}H NMR of AMCS). In addition, the chemical shift value at δ 6.93 ppm belongs to aldehyde amine linked proton, i.e., HC=NCS hydrogen, δ 3.82 ppm number signal corresponded to NH attached methylene protons and carbonyl connected methylene protons shift at the value of δ 3.18 ppm. Moreover, the other spectral values in Fig. 3F (^{1}H NMR of AMCS) were related to the chitosan group protons.

3.1.5. *^{13}C NMR analysis*

On the other hand, the Carbon ^{13} NMR spectrum of the CS and AMCS is shown in Fig. 4A and B. There were three carbonyl carbon peaks observed in the spectra, the signal at δ 169.9, 171.8 and 178.1 ppm related to carbons of CONHNH, H_2NCONH and HNCSN. This means that these three peaks revealed the formation of the final chitosan modification product. In fact, the other chemical shits are associated with δ 42.6 ($NHNHCH_2$), 44.7 ($HNCH_2$), 56.6 (CH_2CO) and 158.2 (N=CH). While the aromatic benzene carbons peak ranges from δ 127.5 to 140.6 ppm. Meanwhile, the remaining peaks belong to chitosan carbons.

3.2. *Point of zero charge (pH_{PZC})*

The solid addition approach was used to identify the pH_{PZC} of AMCS. For that, NaOH and HCl (0.1 M) solutions were used to alter a 0.01 M solution of NaCl (30 mL) in 50 mL conical flasks to various pH values of 1.0 to 10.0 (the initial pH, pH_i). Subsequently, precisely 0.5 g of AMCS was introduced to several flasks and incubated for 24 h at 200 rpm in a shaking incubator at 298 K. Every flask's pH was tested after incubation and noted as the final pH (pH_f). Plotting the variance between the pH_i and pH_f values against the original pH data yielded the following result: $\Delta pH = pH_f - pH_i$. Plotting the curves at zero pH and crossing them with the X-axis will yield the pH_{PZC} value. From Fig. 5A, the pH_{PZC} of the AMCS is 5.3. When the pH is lower than the pH_{PZC}, the AMCS surface becomes positively charged due to the protonation of amine groups. Conversely, when the pH exceeds the pH_{PZC}, the surface of AMCS becomes negatively charged as a result of deprotonation.

3.3. *Influence of solution pH*

pH performs a vital role throughout the sorption process. It can regulate the surface charge of the biosorbent and the ionization of the sorbate in the solution as well as the dissociation of functional groups. The impact of pH on U(VI) removal was examined from 1.0 to 10.0 (Fig. 5B) at 298 K with a constant U(VI) concentration (50 mg/L). The concentration of H^+ ions is very high at lower pH values. In most cases, the protons can easily protonate with amine groups to form $-NH_3^+$, and it will also affect the sorption uptake of the AMCS. Hence, the number of active binding sites will be reduced, and there will be competition between the H^+ and UO_2^{2+} ions. Upon raising the solution pH, the difference in U(VI) sorption is generally due to changing U(VI) species. The % removal of U(VI) onto AMCS rises with the rising pH from 2.0 to 5.0. The U(VI) removal efficiency by AMCS strongly depends on variations of the solution pH, and the removal percentage of U(VI) rises with rising pH to a maximal value (pH 5.0). At low pH values, uranium predominantly exists as free uranyl ions ($UO2^{2+}$) in solution. At low pH, uranium is primarily found as the free uranyl ion (UO_2^{2+}) in solution. As pH increases, uranyl ions undergo hydrolysis, forming hydrolyzed species such as ($(UO_2)_2(OH)_2)^{2+}$, $[(UO_2)_3(OH)_5)^+$). These species, predominantly present between pH 4 and 6, remain positively charged and can interact with negatively charged adsorbents. With further increases in pH, U(VI) generates anionic hydroxyl complexes, including $UO_2(OH)_3^-$, $UO_2(OH)_4^{2-}$ and $(UO_2)_3(OH)_7^-$, as well as soluble carbon complexes like $UO_2(CO_3)_2^{2-}$ and $UO_2(CO_3)_3^{4-}$ [45–47]. Above pH 5, negatively charged hydrolyzed species begin to dominate the system, leading to reduced interaction with highly negatively charged adsorbent materials. This decline in interaction is primarily attributed to electrostatic repulsion from the coexisting anions resulting from uranyl hydrolysis, consequently decreasing the overall uptake of uranium. Moreover, with an increase in the pH (>5), the AMCS surface becomes increasingly negatively charged due to deprotonation, rendering it less capable of adsorbing the U(VI) ions. Therefore, for further U(VI) removal tests, pH 5.0 is considered to be the ideal pH. Similar results were found for the pH solutions effect using different adsorbents on the removal of U(VI) [27,48,49].

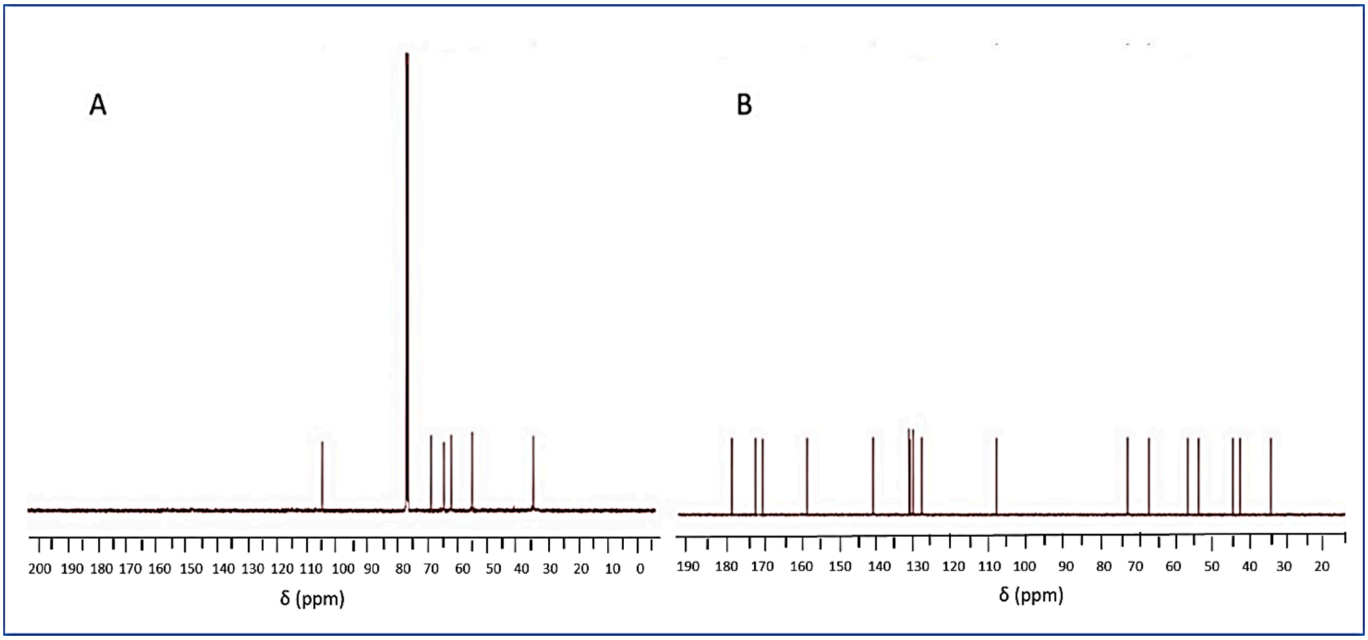

Fig. 4. ^{13}C NMR spectra of (A) CS and (B) AMCS.

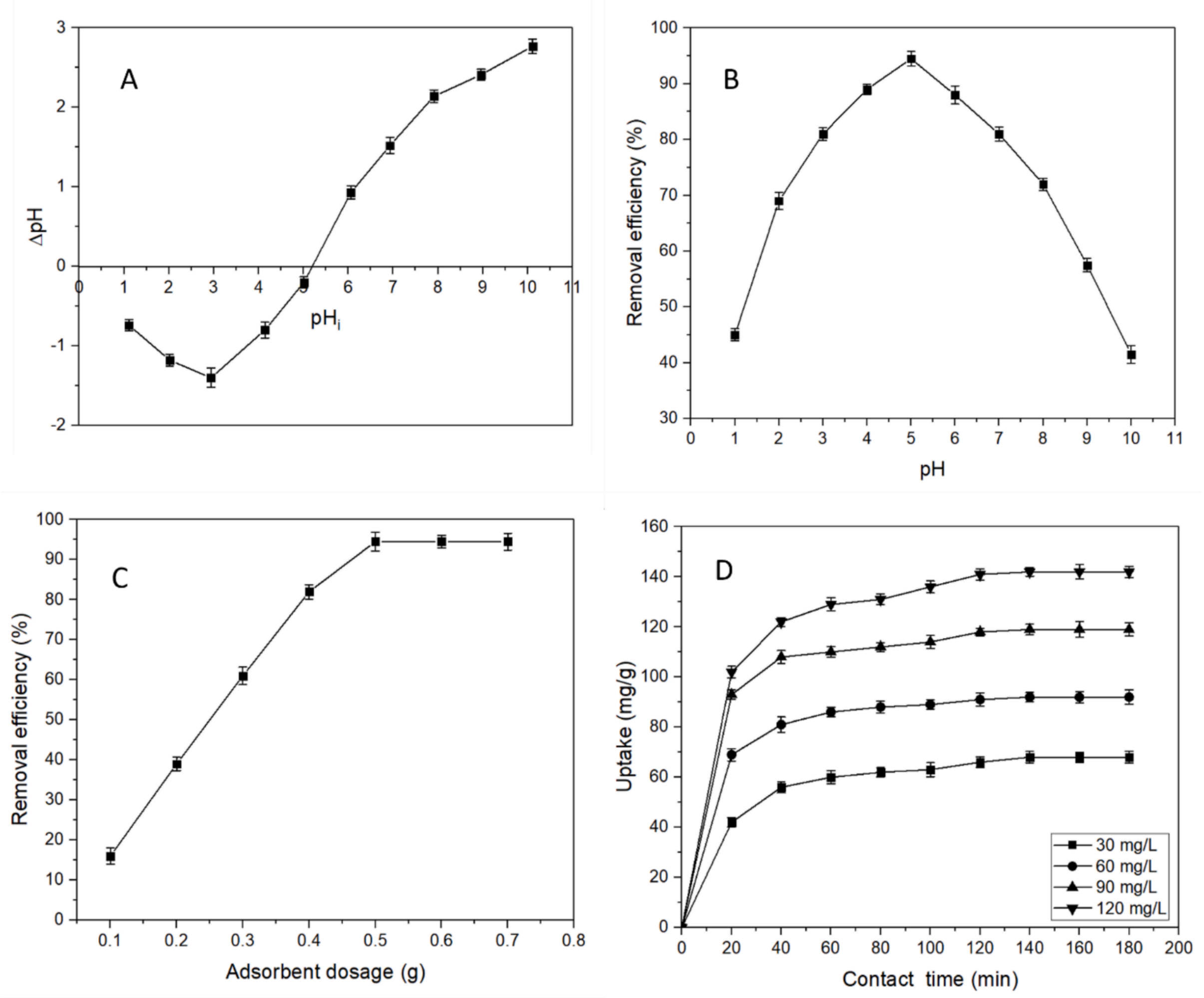

Fig. 5. (A) point of zero charge (pH_{PZC}) [pH = 1 to10; electrolyte volume = 30 mL; temperature = 298 K; dosage = 0.5 g; speed = 200 rpm; error bars represent ± SD (n = 2)]; (B) effect of pH [pH = 1 to10; C_i = 50 mg/L; V = 30 mL; dosage = 0.5 g; temperature = 298 K; time = 140 min; speed = 200 rpm; error bars represent ± SD (n = 2)]; (C) adsorbent dose [dosage = 0.1–0.7 g; pH = 5.0; C_i = 50 mg/L; V = 30 mL; temperature = 298 K; time = 140 min; speed = 200 rpm; error bars represent ± SD (n = 2)]; and (D) contact time [time duration = 0–180 min; pH = 5.0; C_i = 30–120 mg/L; V = 30 mL; temperature = 298 K; speed = 200 rpm; dosage = 0.5 g; error bars represent ± SD (n = 2)] on the removal of U(VI) onto AMCS.

3.4. *Influence of AMCS dose*

In the sorption process, the dose is a significant parameter that assesses the adsorbent's sorption ability for a particular initial concentration. The impact of dose studies was performed by changing the AMCS mass from 0.1 to 0.7 g with a 50 mg/L concentration of U(VI), as displayed in Fig. 5C. U(VI) removal percentage rises with an enhancement of AMCS quantity from 0.1 g to 0.5 g. This clearly indicates that the maximum adsorption is achieved at 0.5 g. The pattern that has been shown indicates that as the amount of adsorbent grows, so does the adsorptive surface area, making more active sites available for adsorption. After that, (over 0.5 g), it became nearly stable because huge doses of the adsorbent inhibited or overlapped its active areas. The above findings show that 0.5 g was the ideal dose for all further tests. The same phenomenon was reported by Solgy et al. [50].

3.5. *Influence of contact time*

Experiments on contact time were performed by changing the time from 0 to 180 min at room temperature under constant pH 5.0, 0.5 g of sorbent quantity, and 30–120 mg/L of adsorbate concentration solution. Contact duration influence on the sorption efficiency of U(VI) ions was examined by separating the supernatant at various time intervals (0 to 180 min) and the results acquired are displayed in Fig. 5D. The contact time experiments reveal that the sorption capacity rises rapidly in the first 20 min, and thereafter it remains constant until attaining adsorption equilibrium at 140 min. At the initial stage, the active surface sites were sufficient; hence, the adsorption rate was fast, and there was a strong interaction between the AMCS and the U(VI). Because of attractive electrostatic attractions, the Van Der Waals strength and rapid diffusion on the internal face of the adsorbent led to this adsorption. With increasing time, more effective sites were surrounded with the U (VI) ions, and the adsorption reached equilibrium at a particular time. No significant changes in the adsorption uptake of the AMCS beyond the optimum contact time. For further batch sorption experiments, the reaction time of 140 min was chosen as an optimal contact time. Similar results were observed in other studies [42,51].

3.6. *Adsorption kinetic modelling*

The kinetic analysis gives a clear idea of the conditions of sorbent-sorbate interactions. Pseudo-first-order (PFO) [52] and pseudo-second-order (PSO) [53] models are applied to determine the kinetic data of the reaction.

$$q_t = q_{e1}(1 - exp(-k_1 t)) \quad (5)$$

where q_e (mg/g) is the quantity of U(VI) sorbed at equilibrium. k_1 represents the PFO rate constant. Table 1 summarizes the obtained kinetic parameters (K_1 values) and coefficient values (R^2) of the PFO. It can be clearly noticed that the correlation coefficients (R^2 values) of the PFO kinetic model were lower than those of the PSO model. The contrast between experimental ($q_{e,\exp}$) and calculated ($q_{e,cal}$) values indicates that the PFO model did not accept U(VI) sorption well. Furthermore, the χ^2 and SSE values of PFO are high compared to PSO (Table 1).

$$q_t = \frac{q_{e2}^2 k_2 t}{1 + q_{e2} k_2 t} \tag{6}$$

where k_2 represents the rate constant of the PSO. q_t (mg/g) is the quantity of U(VI) sorbed at time t. The non-linear PFO and PSO kinetic models are shown in Fig. 6 with different U(VI) concentrations. The values of k_2 are presented in Table 1. It is apparent that the PSO kinetic model R^2 values were more significant than the PFO model. For the PSO model, the calculated ($q_{e,\ cal}$) values are much closer to the experimental ($q_{e,\ \exp}$) values. Furthermore, the PSO model displayed lower χ^2 and SSE values when compared to the PFO model (Table 1). These findings show that the PSO model is more desirable for eliminating U(VI) adsorption onto AMCS.

The intra-particle diffusion (IPD) model, proposed by Weber-Morris [54], was applied via Eq. (7) to explore the diffusion mechanism of the process.

$$q_{t=k_{id}t^{0.5}+C} \tag{7}$$

here, k_{id} (mg/g min$^{0.5}$) is the IPD rate constant, and the constant C (mg/g) indicates resistance to mass transfer in the boundary layer. The values of IPD, k_{id}, were derived from the graph depicting U(VI) uptake, q_t, plotted against $t^{0.5}$ at various concentrations, as shown in Fig. 7. These values can be found in Table 2. The experimental data for all concentrations demonstrate multi-linear plots, indicating that IPD plays a role in the sorption process. The non-zero intercepts of the straight lines ($C \neq 0$) suggest that IPD is not the only rate-limiting step and that film diffusion may also contribute to the adsorption kinetics [55]. In Table 2, the diffusion rate constants in all plots follow the decreasing order: $k_{id,1} > k_{id,2} > k_{id,3}$. The initial stages, which are the steepest portions of the graphs, indicate the presence of fresh active sites on the AMCS surface. As U(VI) ions occupy the exterior active sites, they attempt to penetrate the adsorbent pores and become adsorbed by the interior surfaces [56]. Consequently, the adsorption rate gradually decreases in the later stages of the curves. In the final stage's equilibrium condition, the deficient U(VI) concentrations significantly reduce IPD. On the other hand, the k_{id} values surge with the initial U(VI) concentration, possibly due to the increasing driving force, leading to decreased U(VI) diffusion in the boundary layer and enhanced diffusion in the solid [55].

3.7. Adsorption isotherms

The adsorbent capability can be defined through sorption isotherms, and the adsorption mechanism can be explored much more carefully. In order to evaluate and design the adsorption systems, it is essential to develop the most adequate correlations for the batch equilibrium information by using scientific or theoretical equations. The Langmuir [57], Freundlich [58] and Sips [59] isotherms are the most popular isotherms to describe solid–liquid sorption processes.

3.7.1. Langmuir isotherm

A fundamental supposition of the Langmuir hypothesis is that the sorption occurs on the surface of the sorbent at specific homogeneous locations. Then, it assumes that no further sorption can occur on this site once a sorbate molecule occupies a particular site. The following equation represents the Langmuir.

$$q_e = \frac{q_m K_L C_e}{1 + K_L C_e} \tag{8}$$

Here, q_e (mg/g) indicates the equilibrium sorption uptake for U(VI), q_m (mg/g) is the maximal equilibrium sorption uptake, K_L (L/mg) is the Langmuir constant, and C_e (mg/L) corresponds to the final U(VI)concentration in the solution. The q_{max} value rose from 287.7 to 305.4 mg/g as the temperature rose from 298 to 318 K. This enhancement in adsorption uptake can be linked to an elevation in the kinetic energy of the adsorbent particles caused by the temperature rise. The rise in kinetic energy leads to a higher frequency of collisions between the sorbent and the sorbate, which results in improved sorption onto the sorbent's surface.

3.7.2. Freundlich isotherm

The Freundlich model, which is based on a heterogeneous surface, can be represented by the following Eq.:

$$q_e = K_f C_e^{1/n} \tag{9}$$

Here, q_e (mg/g) denotes the quantity of U(VI) adsorbed per unit mass of sorbent, while C_e (mg/L) represents the final concentration. The parameters n and K_f are the Freundlich exponent and Freundlich constant, respectively, with K_f reflecting the uptake of AMCS and $1/n$ indicating the sorption intensity of AMCS. For U(VI) adsorption, the $1/n$ value lies between 0 and 1, revealing that the system was favourable below-studied conditions.

3.7.3. Sips isotherm

The sips isotherm combines aspects of the Langmuir and Freundlich isotherms and is employed to explain adsorption processes occurring at specific localized adsorption sites where there is minimal interaction between the adsorbate and adsorbent. The following equation can express this model:

$$q_e = \frac{q_m (K_{sC_e})^{n_s}}{1 + (K_{sC_e})^{n_s}} \tag{10}$$

where q_m is the Sips adsorption uptake (mg/g), K_s is the Sips constant ($(\mathrm{L/mg})_s^n$), and n_s is the Sips heterogeneity factor. The n_s value below 1.0 suggests that the biosorbent binding sites were predominantly homogeneous. In the present study, the n_s values are below one, confirming homogeneous adsorption sites in the biosorption of U(VI) ions.

The isotherm fitting plots are presented in Fig. 8, and the corresponding model variables are listed in Table 3. As shown in Table 3, the Langmuir model exhibited the highest correlation coefficient ($R^2 > 0.9991$), indicating a better fit to the experimental data compared to the Sips and Freundlich models. Additionally, the Langmuir model yielded the lowest values of χ^2 and SSE, further confirming its superior

Table 1
Pseudo-first-order and pseudo-second-order model constants for the adsorption of U(VI) onto AMCS.

Adsorbent	U(VI) Conc. (mg/L)	$q_{e,\exp}$ (mg/g)	Pseudo-first-order					Pseudo-second-order				
			$q_{e,cal}$ (mg/g)	k_1 (L/min)	R^2	χ^2	SSE	$q_{e,cal}$ (mg/g)	k_2 (g/mg. min)	R^2	χ^2	SSE
AMCS	30	72.6	66.2	0.0508	0.9879	8.649	2.541	73.3	0.0011	0.9988	2.009	0.230
	60	98.1	90.6	0.0670	0.9886	7.674	3.588	97.4	0.0013	0.9995	3.231	0.319
	90	120.4	115.3	0.0800	0.9862	10.430	4.269	121.9	0.0014	0.9997	0.886	0.094
	120	147.1	138.6	0.0901	0.9893	6.805	2.012	150.8	0.0017	0.9986	2.486	0.125

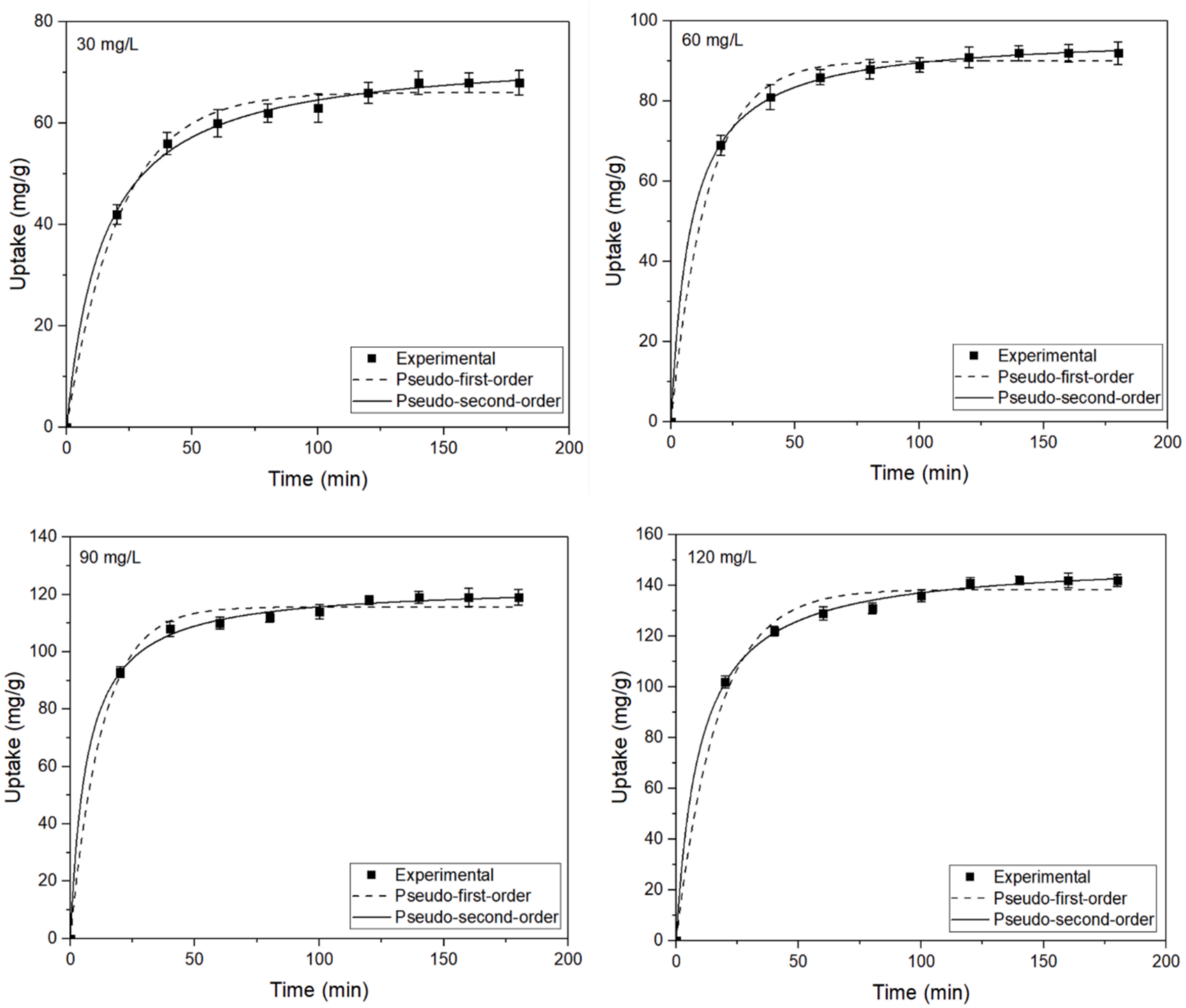

Fig. 6. Non-linear pseudo-first-order and pseudo-second-order kinetic plots for U(VI) onto AMCS at different concentrations [time duration = 0–180 min; pH = 5.0; C_i = 30–120 mg/L; V = 30 mL; temperature = 298 K; speed = 200 rpm; dosage = 0.5 g; error bars represent ± SD (n = 2)].

applicability. Therefore, the U(VI) sorption onto AMCS follows the Langmuir model more closely. The overall order of model fit to the experimental data is: Langmuir > Sips > Freundlich.

3.8. *Thermodynamic analysis*

Assessing thermodynamic variables is crucial to predicting the adsorption process's mechanism and feasibility. The thermodynamic factors, such as ΔG^o (Gibbs free energy change), ΔH^o (enthalpy change), and ΔS^o (entropy change), were calculated using the following Eqs. [60,61]:

$$K_e = \frac{1000 \times K_g \times M_{adsorbate} \times [adsorbate]^0}{\gamma} \tag{11}$$

$$lnK_e = -\left(\frac{\Delta H^o}{RT}\right) + \left(\frac{\Delta S^o}{R}\right) \tag{12}$$

$$\Delta G^o = -RTlnK_e = \Delta H^o - T\Delta S^o \tag{13}$$

where K_e is the equilibrium constant (dimensionless), γ represents the activity coefficient of adsorbate, $M_{adsorbate}$ (g/mol) denotes the molar mass of adsorbate, K_g (L/mg) is the constant associated with the fitted isotherm model, $[adsorbate]^0$ (mol/L) is the standard concentration, R (8.314 kJ/mol K) is the gas constant, and T denotes the temperature. If

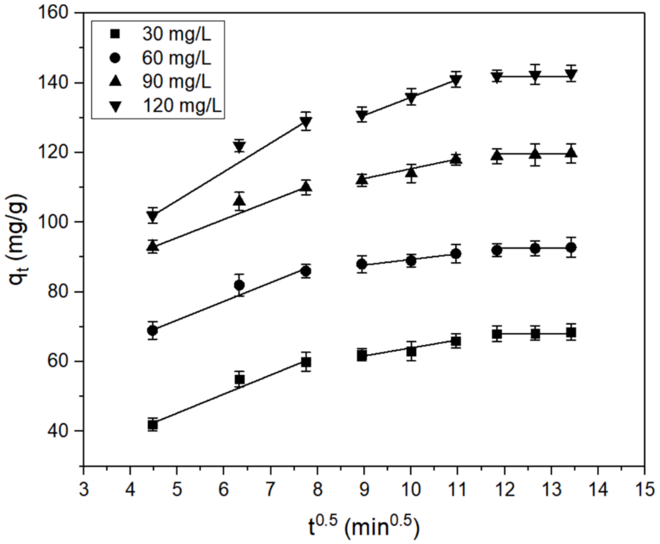

Fig. 7. Intra-particle diffusion model plots for U(VI) onto AMCS at different initial concentrations [pH = 5.0; C_i = 30–120 mg/L; temperature = 298 K; dosage = 0.5 g; error bars represent ± SD (n = 2)].

Table 2
Parameter of fitted IPD model during stages I, II and III at different concentrations.

U(VI) Conc. (mg/L)	Stage 1					Stage II					Stage III				
	$k_{id,1}$ (mg/g $min^{0.5}$)	C_1 (mg/g)	R^2	χ^2	*SSE*	$k_{id,2}$ (mg/g $min^{0.5}$)	C_2 (mg/g)	R^2	χ^2	*SSE*	$k_{id,3}$ (mg/g $min^{0.5}$)	C_3 (mg/g)	R^2	χ^2	*SSE*
30	4.383	17.9	0.9696	15.3	4.32	1.148	44.1	0.9069	21.3	11.14	0.315	64.3	0.9824	12.3	5.82
60	5.283	46.3	0.9521	18.4	6.45	1.972	74.6	0.9527	19.32	7.42	0.442	86.1	0.9844	11.6	4.74
90	5.573	70.4	0.9586	21.3	6.01	2.966	85.1	0.9622	16.32	5.43	0.506	113.2	0.9987	2.3	0.46
120	8.373	65.9	0.9624	16.4	5.49	4.971	86.5	0.9992	3.41	1.24	0.642	136.8	0.9959	7.7	1.49

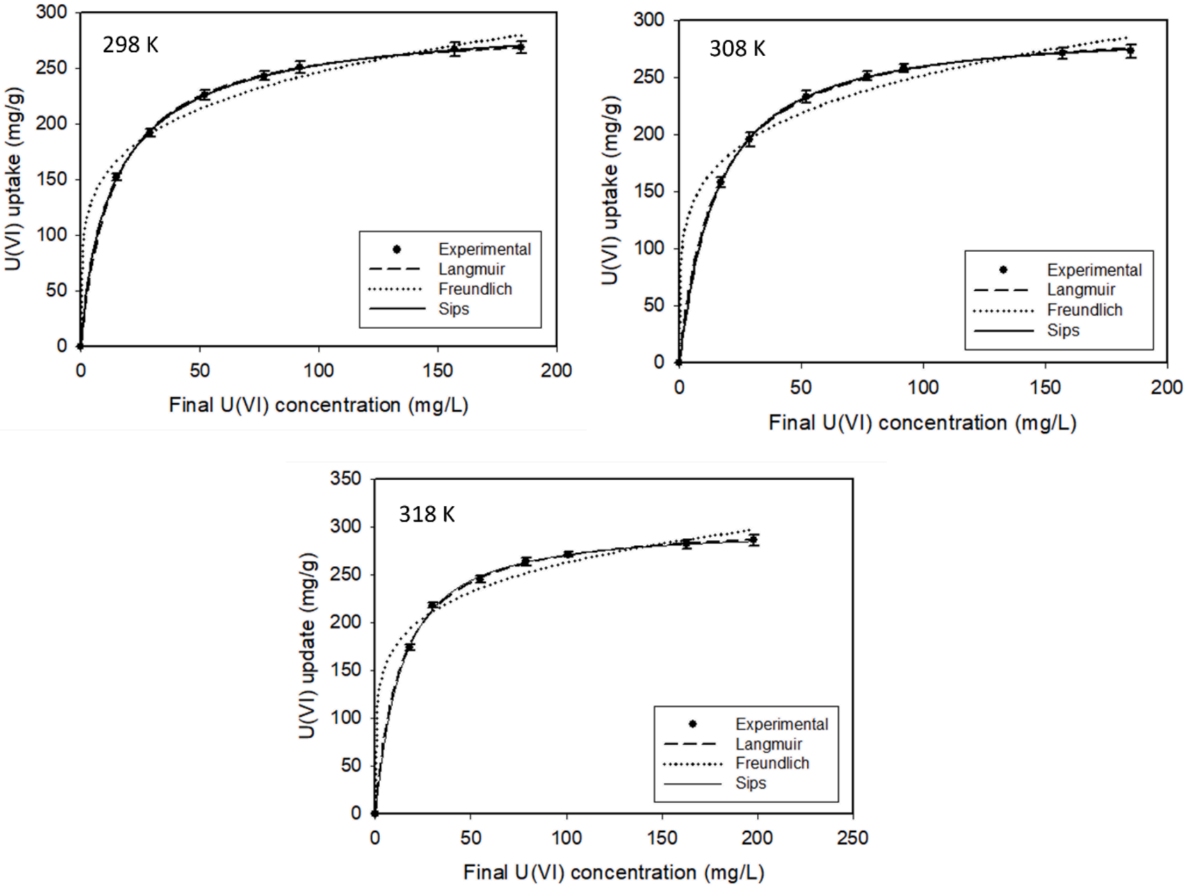

Fig. 8. Non-linear adsorption isotherms plots for U(VI) onto AMCS at different temperatures [temperature = 298–318 K; V = 30 mL; speed = 200 rpm, time = 140 min; pH = 5.0; dosage = 0.5 g; error bars represent ± SD (n = 2)].

ΔG^o values are between −20 and 0 kJ/mol, then the mechanism should be physisorption, but the values in a range of −80 to −400 kJ/mol, the mechanism is chemisorption and the values in a range of −20 to −80 kJ/mol refers the physisorption together with chemisorption [62]. ΔG^o had negative values (Table 4) and demonstrated that U(VI) adsorption was spontaneous at the studied temperatures (298–318 K). Decreasing the value of ΔG^o with the temperature rise suggests favourable U(VI) adsorption. In addition, the value of ΔH^o can decide whether U(VI) sorption was physical or chemical sorption. If ΔH^o is within a range of 2.1–20.9 kJ/mol physisorption occurs, and chemisorption occurs between 20.9 and 418.4 kJ/mol. Positive ΔH^o value (Table 4) illustrates the endothermic existence of U(VI) onto AMCS. The measured ΔH^o values suggest that the elimination of U(VI) onto AMCS was achieved by physisorption. Positive ΔS^o value (Table 4) reveals the raised randomness at the solid-solution interface during U(VI) removal onto AMCS. The thermodynamic study is shown in Fig. 9.

3.9. *Regeneration and reusability of AMCS*

Recycling biosorbent materials is advantageous as it helps reduce operational adsorption costs and the extraction of U(VI) from liquid solutions. Fig. 10A illustrates how varying NaOH eluent concentration affects the U(VI) adsorption from AMCS. As indicated in Fig. 10A, the desorption efficiency decreased from 93.5 % to 51.2 % when applying eluent concentrations of 0.1 M NaOH and 0.4 M NaOH, respectively. This indicates that more substantial concentrations of NaOH are detrimental to the desorption of U(VI) due to the damage to the active sites on the surface of AMCS. Consequently, a 0.1 M NaOH eluent was selected for the regeneration study, as this concentration provided the highest U(VI) recovery during desorption. The reusability of AMCS was assessed based on its adsorption–desorption performance, as demonstrated in Fig. 10B. In the first step, an efficacy of 93.36 % U(VI) recovery was achieved with 0.1 M NaOH; thus, this concentration is ideal for adsorbent regeneration. U(VI) recovery percentage decreases gradually, increasing the number of cycles. The adsorption potential reduced from 91.36 to 76.32 %, and the recovery of U(VI) ions reduced from 91.25 %

Table 3
Langmuir, Freundlich, and Sips isothermal constants for U(VI) adsorption onto AMCS at different temperatures.

Name of the Isotherm	Parameters	298 K	308 K	318 K
Langmuir	q_m (mg/g)	287.7	293.6	305.4
	K_L (L/mg)	0.0705	0.0748	0.0797
	R^2	0.9995	0.9991	0.9996
	χ^2	11.2	12.6	9.7
	SSE	6.8	7.2	4.5
Freundlich	K_f (mg/g)	98.5	99.19	115.25
	n	5.0512	4.9496	5.586
	R^2	0.9882	0.9889	0.9868
	χ^2	124.2	133.6	147.9
	SSE	56.3	47.8	65.3
Sips	q_m *(mg/g)*	52.19	31.53	17.09
	K_s *(L/g)*$_s^{\beta}$	0.1538	0.1029	0.0572
	n_s	0.6340	0.7841	0.9273
	R^2	0.9965	0.9987	0.9992
	χ^2	15.6	13.3	11.9
	SSE	9.4	8.7	7.1

Table 4
Thermodynamic parameters of U(VI) onto AMCS.

Temperature (K)	ΔG^o (kJ/mol)	ΔH^o (kJ/mol)	ΔS^o (J/mol K)
298	−25.146	4.698	100
308	−26.131		
318	−27.149		

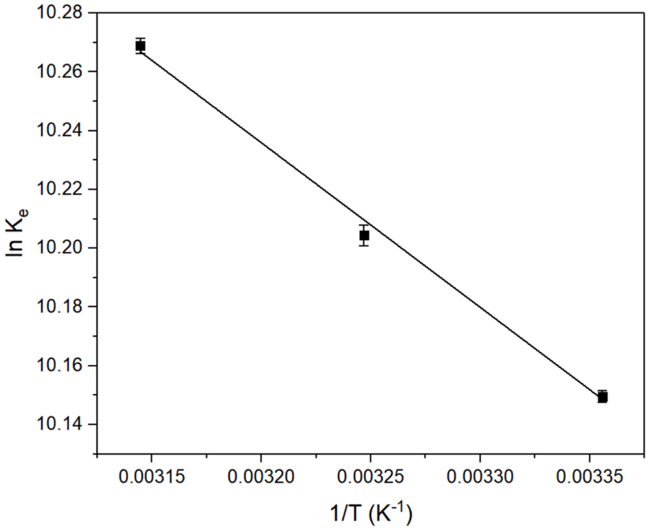

Fig. 9. Linear plot of *1/T* vs. lnK_e for the estimation of thermodynamic parameters for U(VI) adsorption onto AMCS [temperature = 298–318 K; volume = 30 mL; speed = 200 rpm, pH = 5; dosage = 0.5 g; error bars represent ± SD (n = 2)].

(1st cycle) to 72.22 % (4th cycle). The % of U(VI) adsorption and U(VI) desorption reduced slightly from the first to the fourth cycle. The results revealed that AMCS can be frequently used as an adsorbent with minimal loss of the total adsorption power in U(VI) adsorption studies.

3.10. *Application of real uranium wastewater analysis*

The extraction of uranium from mines and the operation of nuclear power plants inevitably lead to the risk of nuclear leakage, producing radioactive wastewater that poses serious threats to both environmental and human health. To assess the practical applications of AMCS in the removal of uranium, we conducted removal experiments using actual wastewater from a uranium mining facility in southern China. The samples exhibited uranium concentrations of 1.43, 1.72, and 2.12 mg/L, with corresponding pH values of 3.2, 3.4, and 3.2. Experimental conditions were maintained without pH adjustment to reflect real-world scenarios. It is important to note that the initial pH of the uranium solutions significantly influences the adsorption dynamics; variations in pH alter both the morphology of uranyl ions and the surface charge characteristics of the adsorbent. Adsorption tests were performed with a dosage of 0.5 g of AMCS. The removal efficiencies achieved were impressively high, recorded at 62.13 %, 73.24 %, and 65.33 % across the different uranium concentrations and the obtained results were depicted in Fig. 11. These findings suggest that AMCS exhibits considerable potential for the in-situ treatment of uranium wastewater, offering both economic feasibility and effective performance.

3.11. *AMCS compared to other biosorbents*

Table 5 compares AMCS sorption efficiency for removing U(VI) with other biosorbents [27,32,63–72]. The table shows that AMCS has broad adsorption potential, and its biodegradability and reusability are some of its advantages in U(VI) removal. Compared to the adsorbents listed in Table 5, the value of q_{max} for U(VI) adsorption onto AMCS is much higher. The other sorbents have considerably lower adsorption potential, which may be due to less surface area, pore size, pore volume, and availability of functional groups in the sorbent. In Fig. 12A, the study clearly explains how U(VI) interacts with the AMCS, and the results support that AMCS is more competitive than other adsorbents in U(VI) removal. It is worth noting that AMCS effectively removes U(VI) from the aqueous medium.

3.12. *Adsorption mechanism*

The adsorption mechanism of U(VI) was investigated through FTIR and SEM, along with elemental mapping analysis. As displayed in Fig. 2, the U(VI) that was adsorbed is evenly spread across the AMCS surface, indicating that U(VI) adsorption is uniform. Additionally, the distribution patterns of the elements U, O, S, and N show similarities on the AMCS surface, implying that the N, O, and S functional groups are the primary sites for U(VI) adsorption. U(VI) can interact with nitrogen, allowing it to share electron pairs with UO_2^{2+} to create complexes that facilitate adsorption. These results indicate that nitrogen-containing functional groups contribute to the sorption process. Based on the analysis provided, the adsorption of uranium by AMCS is influenced by several mechanisms, mainly chemisorption with some degree of physisorption, and its mechanism is illustrated in Fig. 12B. Uranyl ions may form a complex by coordinating with two nitrogen donors from amine groups and two oxygen donors from hydroxyl groups. U(VI) sorption can occur through different mechanisms depending on the pH. Under acidic conditions, the generated AMCS surfaces become deprotonated, which allows uranium ions to be adsorbed onto the AMCS surface via electrostatic attraction. FTIR analysis indicated that AMCS possesses several functional groups on its surface, including –OH and –O, which may serve as active sites for U(VI) ions through ion exchange. The interaction between U(VI) and the functional groups of AMCS is described as a monolayer chemical sorption process, supported by the accurate fitting of the Langmuir model for the isotherms and the PSO model for the kinetics.

4. Conclusions

Economically feasible and environmentally friendly biosorbents with high sorption capacities are necessary for removing U(VI) pollutants from aqueous solutions and polluted samples. In this research, AMCS was synthesized using the crosslinking method, and it was characterized

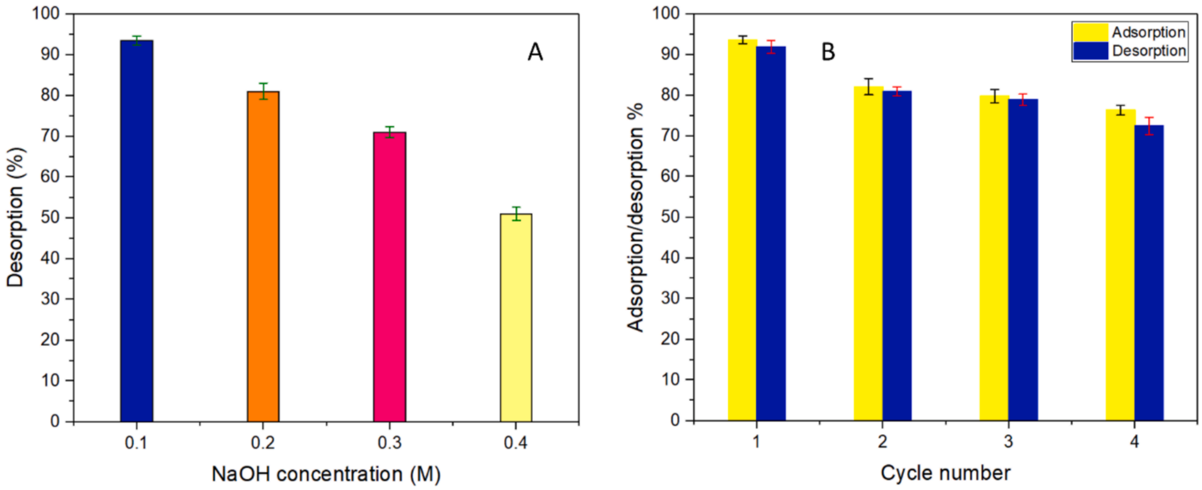

Fig. 10. (A) Desorption % of NaOH at different concentrations [NaOH concentration = 0.1–0.4 M; volume of eluent = 30 mL; dosage = 0.5 g; temperature = 298 K; time = 140 min; speed = 200 rpm; error bars represent ± SD (n = 2)] and (B) Adsorption-desorption cycles of U(VI) onto AMCS [V = 30 mL; dosage = 0.5 g; temperature = 298 K; time = 140 min; speed = 200 rpm; error bars represent ± SD (n = 2)].

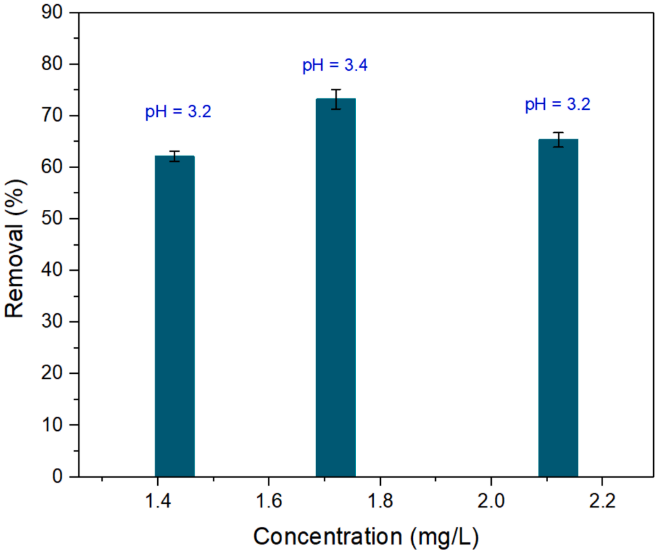

Fig. 11. The removal of U(VI) in different concentrations of real wastewater samples [V = 30 mL; dosage = 0.5 g; temperature = 298 K; time = 140 min; speed = 200 rpm; error bars represent ± SD (n = 2)].

using various techniques such as BET, FTIR, and SEM with elemental mapping, as well as ^{1}H NMR and ^{13}C NMR spectral analysis. The effect of several batch process variables, including solution pH (2–10), AMCS dosage (0.1–0.7 g), contact time (0 to 180 min), and temperature (298, 308 and 318), was investigated for U(VI) elimination. The highest removal efficiency occurred in an acidic solution (pH 5.0; R% = 94.5 %) The adsorption kinetic results indicated that the U(VI) elimination process was well-fitted to the PSO kinetic model ($R^2 > 0.9986$). The outcomes demonstrated that IPD and film diffusion have an impact on the rate-limiting stage of the adsorption process. The isotherms best describe the adsorption equilibrium data in the order: Langmuir > Sips > Freundlich model. The AMCS's maximal U(VI) adsorption uptake was obtained at 287.7 mg/g at 298 K. The thermodynamic variables $\Delta G^o < 0$, $\Delta H^o > 0$, and $\Delta S^o > 0$ reveal that the adsorption of U(VI) on AMCS was spontaneous, endothermic and led to an increase in the system's disorder. The regeneration experiments revealed that AMCS could be effectively desorbed using 0.1 M NaOH. Impressively, it maintained excellent performance over four cycles, underscoring its potential as a reliable and reusable sorbent for the efficient removal of U(VI) from contaminated water. The adsorption mechanism confirmed electrostatic interactions, complexation, and ion exchange between U(VI) and AMCS. This study provides valuable insights into the water treatment field by presenting a sustainable and efficient solution for addressing metal pollution in environmental matrices.

Table 5
Comparison of AMCS adsorption uptake with various adsorbents.

Name of the Adsorbent	pH	Temp. (K)	q_{max} (mg/g)	Reference
MnO_2@PPy	5.0	298	63.04	[27]
Fe-SC4	4.0	298	89.00	[63]
Amidoxime-g-chitosan/bentonite [P(AO)-g-CTS/BT	8.0	298	49.09	[64]
Lysinibacillus-GO	4.5	303	149.30	[65]
Polypyrrole	5.0	298	87.72	[66]
Titanate nanotubes	5.0	298	1.40	[67]
Fe_3O_4@C@MnO_2	5.0	298	77.71	[68]
Amidoxime modified multiwalled carbonnanotubes	5.0	298	67.9	[69]
PVP/chitosan nanofiber	6.0	298	167	[32]
TNTs/ACF	5.0	298	188	[70]
PCT-2	5.0	298	259.91	[71]
PEI-TMC	6.0	298	212.8	[72]
CGPA	6.0	318	263.86	[73]
IPCL-2	5.0	298	278.8	[74]
Chitosan-FeS@biochar	4.16	308	92.45	[75]
PAO/GH	5.0	298	222.2	[76]
CS-EDTA-LDH	5.0	298	272.3	[77]
AMCS	5.0	298	287.7	Present Study

CRediT authorship contribution statement

Venkata Subbaiah Munagapati: Writing – original draft, Visualization, Methodology, Formal analysis, Data curation, Conceptualization. **Hsin-Yu Wen:** Visualization, Validation, Conceptualization. **Anjani R.K. Gollakota:** Formal analysis, Conceptualization. **Jet-Chau Wen:** Writing – review & editing, Supervision, Resources, Funding acquisition, Data curation, Conceptualization. **Kun-Yi Andrew Lin:** Writing – review & editing, Visualization. **Yuvaraja Gutha:** Formal analysis, Data curation, Conceptualization. **Chi-Min Shu:** Writing – review & editing. **Vijaya Yarramuthi:** Validation, Conceptualization.

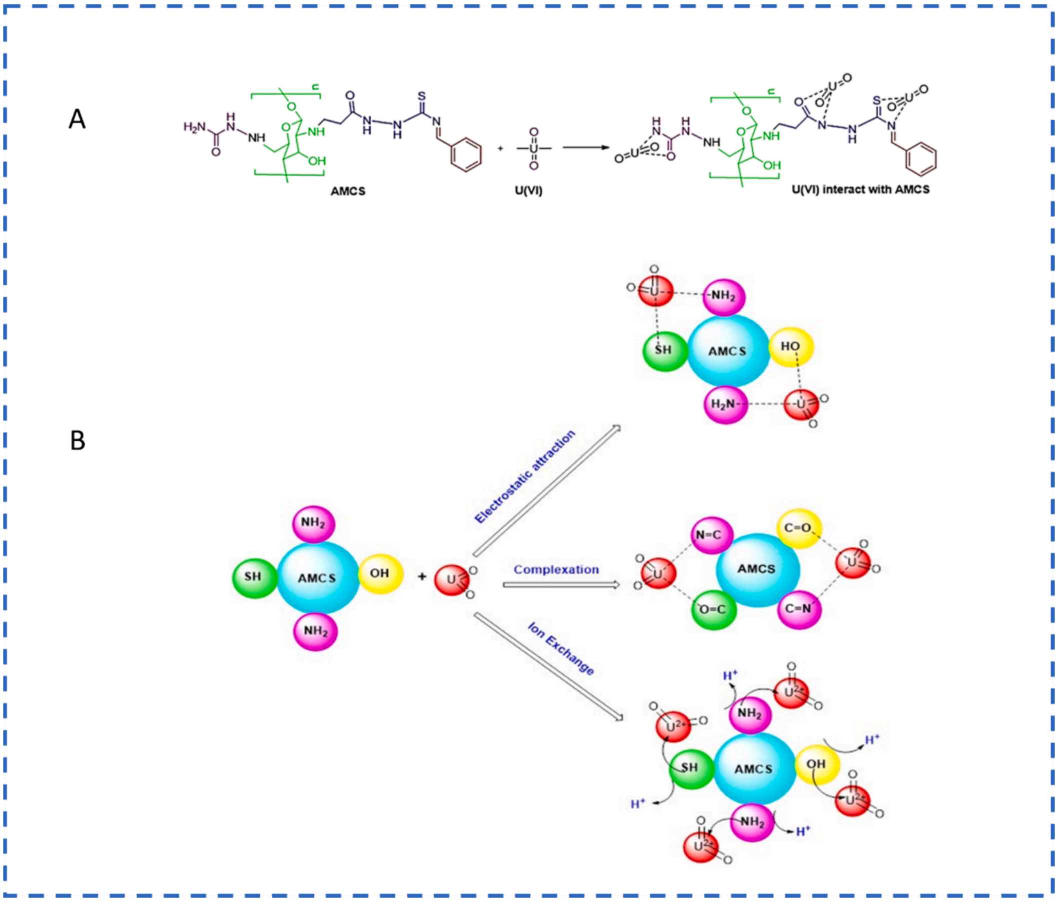

Fig. 12. (A) Interaction of U(VI) ions with the functional groups present in AMCS and (B) Illustration of Functional groups interacting with U(VI) and its sorption mechanism.

Declaration of competing interest

The authors declare that they have no known competing financial interests or personal relationships that could have appeared to influence the work reported in this paper.

Acknowledgements

The authors would like to acknowledge the research support from NSTC 112-2625-M-224-001 by the National Science and Technology Council, Taiwan.

Data availability

Data will be made available on request.

References

[1] D. Ding, Y. Zhao, Y. Chen, C. Xu, X. Fan, Y. Tu, Recent advances in bimetallic nanoscale zero-valent iron composite for water decontamination: Synthesis, modification and mechanisms, J. Environ. Manage. 353 (2024) 120187.

[2] G. Wang, X. Wang, X. Chai, J. Liu, N. Deng, Adsorption of uranium(VI) from aqueous solution on calcined and acid-activated kaolin, Appl. Clay Sci. 47 (2010) 448–451.

[3] S.P. Dubey, A.D. Dwivedi, M. Sillanpaa, Y.N. Kwon, C. Lee, Single-step green synthesis of imine-functionalized carbon spheres and their application in uranium removal from aqueous solution, RSC Adv. 4 (2014) 46114–46121.

[4] X. Lu, D. Zhang, A.T. Reda, C. Liu, Z. Yang, S. Guo, S. Xiao, Y. Ouyan, Synthesis of amidoxime-grafted activated carbon fibers for efficient recovery of uranium(VI) from aqueous solution, Ind. Eng. Chem. Res. 56 (2017) 11936–11947.

[5] Y. Li, S. Wang, X. Wang, Highly selective removal of U(VI) from aqueous solutions by porous nanomaterials, Eco Energy 2 (2024) 205–219.

[6] Y. Xie, L. Yu, L. Chen, C. Chen, L. Wang, F. Liu, Y. Liao, P. Zhang, T. Chen, Y. Yuan, Y. Lu, B. Huang, H. Yang, S. Wang, S. Wang, L. Ma, F. Luo, Y. Liu, B. Hu, H. Wang, D. Pan, W. Zhu, N. Wang, Z. Wang, L. Mao, S. Ma, X. Wang, Recent progress of radionuclides separation by porous materials, Sci. China Chem. 67 (2024) 3515–3577.

[7] Q. Rong, J. Jin, S. Wang, X. Wang, Recent progress of covalent organic frameworks in high selective separation of radionuclides, Carbon Res. 3 (2024) 52.

[8] Q. Meng, L. Wu, T. Chen, Y. Xiong, T. Duan, X. Wang, Constructing the electron-rich microenvironment of an all-polymer-based S-scheme homostructure for accelerating uranium capture from nuclear wastewater, Environ. Sci. Technol. 58 (2024) 15333–15342.

[9] X. Wang, R.M. Li, J.Y. Liu, R.G. Chen, H.S. Zhang, Q. Liu, Z.S. Lia, J. Wang, Melamine modified graphene hydrogels for the removal of uranium(VI) from aqueous solution, New J. Chem. 41 (2017) 10899–10907.

[10] Y. Pan, D. Li, R. Feng, E. Wiens, N. Chen, R. Chernikov, J. Gotze, J. Lin, Uranyl binding mechanism in microcrystalline silicas: a potential missing link for uranium mineralization by direct uranyl co-precipitation and environmental implications, Geochim. Cosmochim. Acta 292 (2021) 518–531.

[11] S.P. Ghuge, A.K. Saroha, Catalytic ozonation of dye industry effluent using mesoporous bimetallic Ru-Cu/SBA-15 catalyst, Process Saf. Environ. Prot. 118 (2018) 125–132.

[12] F. Chen, M. Lv, Y. Ye, S. Miao, X. Tang, Y. Liu, B. Liang, Z. Qin, Y. Chen, Z. He, Y. Wang, Insights on uranium removal by ion exchange columns: The deactivation mechanisms, and an overlooked biological pathway, Chem. Eng. J. 434 (2022) 134708.

[13] A. Ray, E. Mena, A.M. Chavez, F.J. Beltran, F. Medina, Influence of structural properties on the activity of WO$_3$ catalysts for visible light photocatalytic ozonation, Chem. Eng. Sci. 126 (2015) 80–90.

[14] C. Liu, P.C. Hsu, J. Xie, J. Zhao, T. Wu, H. Wang, W. Liu, J. Zhang, S. Chu, Y. Cui, A half-wave rectified alternating current electrochemical method for uranium extraction from seawater, Nat. Energy 2 (2017) 17007–17014.

[15] S.H. Hosseini, A. Rahmani-Sani, Y. Jalalabadi, M. Karimzadeh, A. Hosseini-Bandegharaei, K. Kharghani, A. Allahabadi, Preconcentration and determination of ultra-trace amounts of U(VI) and Th(IV) using titan yellow-impregnated Amberlite XAD-7 resin, Inter. J. Environ. Anal. Chem. 95 (4) (2015) 277–290.

[16] A. Hosseini-Bandegharaei, M.S. Hosseini, Y. Jalalabadi, M. Nedaie, M. Sarwghadi, A. Taherian, E. Hosseini, A novel extractant-impregnated resin containing carminic acid for selective separation and pre-concentration of uranium(VI) and thorium (IV), Inter. J. Environ. Anal. Chem. 93 (2013) 108–124.

[17] R. Wang, Y. Zhao, C. Xu, Y. Liu, W. Wu, D. Zhao, Enhanced removal of Pb^{2+}, Cd^{2+} and Zn^{2+} ions on porous carbon from aqueous solutions by capacitive deionization: Performance study and underlying mechanism, Surf. Interfaces 45 (2024) 103858.

[18] L. Ding, C. Tao, S. Zhang, B. Zheng, Z. Dang, L. Zhang, One-step synthesis of phosphor-rich, silica-enhanced chitosan aerogel for the efficient adsorption of uranium(VI), Int. J. Biol. Macromol. 259 (2024) 129101.

[19] L. Yang, X. Luo, L. Yan, Y. Zhou, S. Yu, H. Ju, Y. Wang, L. Zhang, Efficient selective adsorption of uranium using a novel eco-friendly chitosan-grafted adenosine 5-monophosphate foam, Carbohydr. Polym. 285 (2022) 119157.

[20] Y. Xie, Q. Rong, C. Wen, X. Liu, M. Hao, Z. Chen, H. Yang, G.I.N. Waterhouse, S. Ma, X. Wang, Covalent organic framework with predesigned single-ion traps for highly efficient palladium recovery from wastes, CCS Chem. 6 (2024) 1908–1919.

[21] D. Ding, D. Zhao, N. Zhou, P. Li, J. Chen, J. Huang, Zeolitic imidazolate framework-cellulose loading GR(II)/Cu for efficient Cr(VI) removal over a wide pH range from water: Combined insights of capture performance and potential mechanism analysis, Int. J. Biol. Macromol. 308 (2025) 142461.

[22] G. Yuvaraja, Y. Pang, D.Y. Chen, L.J. Kong, S. Mehmood, M.V. Subbaiah, D.S. Rao, C.M. Pavuluri, J.C. Wen, G.M. Reddy, Modification of chitosan macromolecule and its mechanism for the removal of Pb(II) ions from aqueous environment, Int. J. Biol. Macromol. 136 (2019) 177–188.

[23] M. Vakili, S. Deng, G. Cagnetta, W. Wang, P. Meng, D. Liu, G. Yu, Sep. Regeneration of chitosan-based adsorbents used in heavy metal adsorption: A review, Sep. Purif. Technol. 224 (2019) 373–387.

[24] Y. Nie, S. Deng, B. Wang, J. Huang, G. Yu, Removal of clofibric acid from aqueous solution by polyethylenimine-modified chitosan beads, Front, Environ. Sci. Eng. 8 (2014) 675–682.

[25] V.K. Mourya, N.N. Inamdar, Chitosan-modifications and applications: Opportunities galore, React. Funct. Polym. 68 (2008) 1013–1051.

[26] Y. Sun, Z.Y. Wu, X. Wang, C. Ding, W. Cheng, S.H. Yu, Macroscopic and microscopic investigation of U(VI) and Eu(III) adsorption on carbonaceous nanofibers, Environ. Sci. Technol. 50 (2016) 4459–4467.

[27] W. Yao, Y.H. Wu, H.W. Pang, X.X. Wang, S.J. Yu, X.K. Wang, In-situ reduction synthesis of manganese dioxide@polypyrrole core/shell nanomaterial for highly efficient enrichment of U(VI) and Eu(III), Sci. China Chem. 61 (2018) 812–823.

[28] T.S. Anirudhan, G.S. Lekshmi, F. Shainy, Synthesis and characterization of amidoxime modified chitosan/ bentonite composite for the adsorptive removal and recovery of uranium from seawater, J. Colloid Int. Sci. 534 (2019) 248–261.

[29] S. Zhuang, R. Cheng, M. Kang, J. Wang, Kinetic and equilibrium of U(VI) adsorption onto magnetic amidoxime-functionalized chitosan beads, J. Cleaner Prod. 188 (2018) 655–661.

[30] M.F. Hamza, J.C. Roux, E. Guibal, Uranium and europium sorption on amidoxime-functionalized magnetic chitosan micro-particles, Chem. Eng. J. 344 (2018) 124–137.

[31] E.A. Imam, I.E.T. El Sayed, M.G. Mahfouz, A.A. Tolba, T. Akashi, A.A. Galhoum, E. Guibal, Synthesis of α-aminophosphonate functionalized chitosan sorbents: Effect of methyl vs phenyl group on uranium sorption, Chem. Eng. J. 352 (2018) 1022–1034.

[32] C. Christou, K. Philippou, T. Krasia-Christoforou, I. Pashalidis, Uranium adsorption by polyvinylpyrrolidone/chitosan blended nanofibers, Carbohyd. Polym. 219 (2019) 298–305.

[33] M.R. Abdi, H.R. Shakur, K. Rezaee, M. Ebrahim Saraee, Sadeghi, Effective removal of uranium ions from drinking water using CuO/X zeolite based nanocomposites: effects of nano concentration and cation exchange, J. Radioan. Nucl. Chem. 300 (2014) 1217–1225.

[34] Z.X. Gu, Y. Wang, J. Tang, J.J. Yang, J.L. Liao, Y.Y. Yang, N. Liu, The removal of uranium (VI) from aqueous solution by graphene oxide–carbon nanotubes hybrid aerogels, J. Radioan. Nucl. Chem. 303 (2015) 1835–1842.

[35] S. Ma, L. Huang, L. Ma, Y. Shim, S.M. Islam, P. Wang, L. Zhao, S. Wang, G. Sun, X. Yang, M.G. Kanatzidis, Efficient uranium capture by polysulfide/layered double hydroxide composites, J. Am. Chem. Soc. 137 (2015) 3670–3677.

[36] Q. Zhang, D. Zhao, S. Feng, Y. Wang, J. Jin, A. Alsaedi, T. Hayat, C. Chen, Synthesis of nanoscale zero-valent iron loaded chitosan for synergistically enhanced removal of U(VI) based on adsorption and reduction, J. Colloid Int Sci. 552 (2019) 735–743.

[37] G. Bayramoglu, M.Y. Arica, Agmatine ligand functionalized magnetic alginate beads for removal of U(VI) ions from solution, J. Radioanal. Nucl. Chem. 333 (2024) 4197–4210.

[38] G. Bayramoglu, M.Y. Arica, Star type polymer grafted and polyamidoxime modified silica coated-magnetic particles for adsorption of U(VI) ions from solution, Chem. Eng. Res. Des. 147 (2019) 146–159.

[39] G. Bayramoglu, S. Tilki, M.Y. Arica, Preparation of amine or carboxyl groups modified cellulose beads for removal of uranium(VI) ions from aqueous solutions, Cellulose 31 (2024) 5133–5149.

[40] G. Bayramoglu, A.G. Cimen, M.Y. Arica, Amidoxime-functionalized magnetic graphene oxide-silica particles for adsorption of U(VI) ions from an aqueous medium, J. Radioanal. Nucl. Chem. 333 (2024) 585–597.

[41] G. Bayramoglu, M.Y. Arica, Polyethylenimine and tris(2-aminoethyl) amine modified p(GA-EGMA) microbeads for sorption of uranium ions: equilibrium, kinetic and thermodynamic studies, J. Radioanal. Nucl. Chem. 312 (2017) 293–303.

[42] G. Yuvaraja, N.C. Zheng, Y. Pang, M. Su, D.Y. Chen, L.J. Kong, S. Mehmood, M. V. Subbaiah, J.C. Wen, Removal of U(VI) from aqueous and polluted water solutions using magnetic Arachis hypogaea leaves powder impregnated into chitosan macromolecule, Int. J. Biol. Macromol. 148 (2020) 887–897.

[43] G. Yuvaraja, D.Y. Chen, J.L. Pathak, J. Long, M.V. Subbaiah, J.C. Wen, C.L. Pan, Preparation of novel aminated chitosan Schiff's base derivative for the removal of methyl orange dye from aqueous environment and its biological applications, Int. J. Biol. Macromol. 146 (2020) 1100–1110.

[44] M. Barjasteh, M. Akrami, S.M. Dehnavi, Fabrication of bacterial cellulose/chitosan-MIL-100(Fe) composite for adsorptive removal of dacarbazine, Int. J. Biol. Macromol. 257 (2024) 128683.

[45] L. Wang, D. Zhao, D. Ding, C. Wu, Y. Chen, Highly improved removal of U(VI) from water by Fe-Cu nanoparticles anchored on corn straw biochar: Influencing factors and mechanism studies, Inorg. Chem. Commun. 153 (2023) 110771.

[46] Q. Zhang, D. Zhao, Y. Ding, Y. Chen, F. Li, A. Alsaedi, T. Hayat, C. Chen, Synthesis of Fe-Ni/graphene oxide composite and its highly efficient removal of uranium(VI) from aqueous solution, J. Clean. Produ. 230 (2019) 1305–1315.

[47] H. Basu, R.K. Singhal, M.V. Pimple, S. Saha, Graphene oxide encapsulated in alginate beads for enhanced sorption of uranium from different aquatic environments, J. Environ. Chem. Eng. 6 (2018) 1625–1633.

[48] M. Ma, Z. Ye, J. Zhang, Y. Wang, S. Ning, X. Yin, T. Fujita, Y. Chen, H. Wu, X. Wang, Synthesis and fabrication of segregative and durable MnO_2@chitosan composite aerogel beads for uranium(VI) removal from wastewater, Water Res. 247 (2023) 120819.

[49] H. Yu, Y. Dai, L. Zhou, J. Ouyang, X. Tang, Z. Liu, A.A. Adesina, Selective biosorption of U(VI) from aqueous solution by ion-imprinted honeycomb-like chitosan/kaolin clay composite foams, Int. J. Biol. Macromol. 206 (2022) 409–421.

[50] M. Solgy, M. Taghizadeh, D. Ghoddocynejad, Adsorption of uranium(VI) from sulphate solutions using amberlite IRA-402 resin: Equilibrium, kinetics and thermodynamics study, Ann. Nucl. Energy 75 (2015) 132–138.

[51] G. Yuvaraja, M. Su, D.Y. Chen, Y. Pang, L.J. Kong, M.V. Subbaiah, J.C. Wen, G. M. Reddy, Impregnation of magnetic-momordica charantia leaf powder into chitosan for the removal of U(VI) from aqueous and polluted wastewater, Int. J. Biol. Macromol. 149 (2020) 127–139.

[52] S. Lagergren, About the theory of so-called adsorption of soluble substances, K. Sven. Vetenskapsakad. Handl. 24 (1898) 1–39.

[53] Y.S. Ho, G. McKay, Pseudo-second order model for sorption processes, Process Biochem. 34 (1999) 451–465.

[54] W.J. Weber, J.C. Morris, Kinetics of adsorption on carbon from solutions, J. Sanity Eng. Div. Amer. Soc. Civ. Eng. 89 (1963) 31–59.

[55] B. Tanhaei, A. Ayati, E. Iakovleva, M. Sillanpaa, Efficient carbon interlayed magnetic chitosan adsorbent for anionic dye removal: Synthesis, characterization and adsorption study, Int. J. Biol. Macromol. 164 (2020) 3621–3631.

[56] Y. Ren, H.A. Abbood, F. He, H. Peng, K. Huang, Magnetic EDTA-modified chitosan/SiO_2/Fe_3O_4 adsorbent: Preparation, characterization, and application in heavy metal adsorption, Chem. Eng. J. 226 (2013) 300–311.

[57] I. Langmuir, The adsorption of gases on plane surfaces of glass, mica and platinum, J. Am. Chem. Soc. 40 (1918) 1361–1403.

[58] H.M.F. Freundlich, Uber die adsorption in lasugen, J. Phys. Chem. 57 (1906) 385–470.

[59] R. Sips, On the structure of a catalyst surface, J. Chem. Phys. 16 (1948) 490–495.

[60] E.C. Lima, A. Hosseini-Bandegharaei, J.C. Moreno-Pirajan, I. Anastopoulos, A critical review of the estimation of the thermodynamic parameters on adsorption equilibria. Wrong use of equilibrium constant in the Van't Hoof equation for calculation of thermodynamic parameters of adsorption, J. Mol. Liq. 273 (2019) 425–434.

[61] A. Naseri, Z. Abed, M. Rajabi, B. Lal, A. Asghari, O. Baigenzhenov, S. Arghavani-Beydokhti, A. Hosseini-Bandegharaei, Use of Chrysosporium/carbon nanotubes for preconcentration of ultra-trace cadmium levels from various samples after extensive studies on its adsorption properties, Chemosphere 335 (2023) 139168.

[62] J.R. Baseri, P.N. Palanisamy, P.S. Kumar, Adsorption of basic dyes from synthetic textile effluent by activated carbon prepared from Thevetia peruviana, Indian, J. Chem. Technol. 19 (2012) 311–321.

[63] L.J. Kong, Y.T. Zhu, M. Wang, Z.X. Li, Z.C. Tan, R.B. Xu, H.M. Tang, X.Y. Chang, Y. Xiong, D.Y. Chen, Simultaneous reduction and adsorption for immobilization of uranium from aqueous solution by nano-flake Fe-SC, J. Hazard. Mater. 320 (2016) 435–441.

[64] T.S. Anirudhan, G.S. Lekshmi, F. Shainy, Synthesis and characterization of amidoxime modified chitosan/bentonite composite for the adsorptive removal and recovery of uranium from seawater, J. Colloid Int. Sci. 534 (2019) 248–261.

[65] C. Zhao, J. Liu, Y. Deng, Y. Tian, G. Zhang, J. Liao, J. Yang, Y. Yang, N. Liu, Q. Sun, Uranium(VI) adsorption from aqueous solutions by microorganism-graphene oxide composites via an immobilization approach, J. Clean. Prod. 236 (2019) 117624.

[66] S. Abdi, M. Nasiri, A. Mesbahi, M.H. Khani, Investigation of uranium(VI) adsorption by polypyrrole, J. Hazard. Mater. 332 (2017) 132–139.

[67] W. Liu, X. Zhao, T. Wang, D. Zhao, J. Ni, Adsorption of U(VI) by multilayer titanate nanotubes: Effects of inorganic cations, carbonate and natural organic matter, Chem. Eng. J. 286 (2016) 427–435.

[68] S. Dai, N. Wang, C. Qi, X. Wang, Y. Ma, L. Yang, X. Liu, Q. Huang, C. Nie, B. Hu, X. Wang, Preparation of core-shell structure Fe_3O_4@C@MnO_2 nanoparticles for efficient elimination of U(VI) and Eu(III) ions, Sci. Total Environ. 685 (2019) 986–996.

[69] J. Wu, K. Tian, J. Wang, Adsorption of uranium (VI) by amidoxime modified multiwalled carbonnanotubes, Prog. Nucl. Energ. 106 (2018) 79–86.

[70] J. Duan, H. Ji, T. Xu, F. Pan, X. Liu, W. Liu, D. Zhao, Simultaneous adsorption of uranium(VI) and 2-chlorophenol by activated carbon fiber supported/modified titanate nanotubes (TNTs/ACF): Effectiveness and synergistic effects, Chem. Eng. J. 406 (2021) 126752.

[71] X. Ao, L. Zhou, J. Jin, Y. Liu, J. Ouyang, Z. Liu, Macroporous and ultralight polyethyleneimine-grafted chitosan/nano-TiO_2 foam as a novel adsorbent with antibacterial activity for the efficient U(VI) removal, Int. J. Biol. Macromol. 253 (2023) 126966.

[72] X. Xie, Y. Wang, W. Zhou, C. Chen, Z. Xiong, Investigation of U(VI) adsorption properties of poly(trimesoyl chloride-co-polyethyleneimine), J. Solid. State Chem. 296 (2021) 121966.

[73] X. Ye, R. Chi, Z. Wu, J. Chen, Y. Lv, C. Lin, Y. Liu, W. Luo, A biomass fiber adsorbent grafted with phosphate/amidoxime for efficient extraction of uranium from seawater by synergistic effect, J. Environ. Manag. 337 (2023) 117658.

[74] H. Wang, L. Zhou, X. Ao, G. Huang, Y. Liu, J. Ouyang, A.A. Adesina, Ion-imprinted macroporous polyethyleneimine incorporated chitosan/layered hydrotalcite foams for the selective biosorption of U(VI) ions, Int. J. Biol. Macromol. 266 (2024) 131113.

[75] G. Chen, H. Wang, L. Han, N. Yang, B. Hu, M. Qiu, X. Zhong, Highly efficient removal of U(VI) by a novel biochar supported with FeS nanoparticles and chitosan composites, J. Mol. Liq. 327 (2021) 114807.

[76] J. Bai, J. Chu, X. Yin, J. Wang, W. Tian, Q. Huang, Z. Jia, X. Wu, H. Guo, Z. Qin, Synthesis of amidoximated polyacrylonitrile nanoparticle/graphene composite hydrogel for selective uranium sorption from saline lake brine, Chem. Eng. J. 391 (2020) 123553.

[77] L. Zhou, H. Zhang, J. Jin, L. Xu, J. Ouyang, X. Ao, A.A. Adesina, Honeycomb-like macroporous crosslinked chitosan assisted EDTA-intercalated Ca-Mg-Al layered hydrotalcite foams for efficient U(VI) biosorption, Int. J. Biol. Macromol. 279 (2024) 135011.

Dr. Venkata SubbaiahMunagapati is a senior post-doctoral researcher at the Research Centre for Soil & Water Resources and Natural Disaster Prevention (SWAN), National Yunlin University of Science and Technology, Douliu, Taiwan. He earned his PhD in 2010 from Sri Venkateswara University, Tirupati, Andhra Pradesh, India. With extensive expertise in environmental science, he has published over 85 research articles in prestigious international journals. His research focuses on wastewater treatment and the development of chemically modified adsorbents and nanocomposites for pollutant removal. Dr. Munagapati has made significant contributions to the field by exploring novel materials for water purification, emphasizing sustainability and efficiency in adsorption processes.

Dr. Hsin-Yu Wen earned her Bachelor's degree in Clinical Medicine from Sichuan University in 2019, followed by a Master's degree in Pathology Department from the same institution. Her research interests encompass a broad range of fields, including Biochemistry and Molecular Biology, Molecular Microbiology and Immunology, Disease Mechanisms, Molecular Pathogenesis, Molecular Medicine, and Biomedical Sciences. Since 2019, Dr. Wen has authored several publications, which have collectively received 159 citations on Google Scholar. In addition to her academic background, she is a licensed physician and has completed her postgraduate year (PGY) training in Pathology.

Dr. Anjani R.K. Gollakota is a chemical engineer with over six years of experience in academia, research, and teaching. Currently serving as a Research Assistant Professor at National Yunlin University of Science and Technology (2018-Present), Dr. Gollakota is passionate about sustainable solutions and inspiring the next generation of engineers. His research expertise lies in metal-organic frameworks, zeolites, coal fly ash utilization, and biofuel upgrading. She has successfully secured research grants and mentored students, contributing to significant research advancements. Dr. Gollakota has authored numerous publications in high-impact journals, showcasing his dedication to scientific inquiry. Key achievements include: Research on converting Taiwan coal residues into novel sorbent materials Designing and synthesizing sorbents to treat dye contaminants Developing ionic liquid functionalized fly ash-based sorbent materials for metal pollutant treatment CFD modeling of bubbles and drops in multiphase flow using ANSYS 14.5 & COMSOL 5.0 Dr. Gollakota's educational background includes a Ph.D. in Chemical Engineering from the Indian Institute of Technology Guwahati (2015), an MBA in Marketing from Pondichisry University (2011), and degrees in Environmental Engineering and Chemical Engineering. His dedication to research and his commitment to fostering the next generation of engineers make his a valuable asset to the scientific community.

Prof. Jet-ChauWen , a life distinguished professor at National Yunlin University of Science and Technology, has dedicated his career to advancing civil and environmental engineering. With academic roots tracing back to Chung Yuan Christian University and a Ph.D. from Utah State University, he has built a legacy of integrating hydrological sciences with sustainable development. His research encompasses hydro-perplexity, Critical Zone science, hydrogeological variability, and innovative groundwater recharge methods. A pioneering effort he led along the Zhuoshui River involved suppressing dust and replenishing groundwater, significantly improving environmental conditions in Yunlin County. Between 2020 and 2023, this initiative contributed 69.33 million tons of recharge and helped sustain agriculture during droughts. Dr. Wen's interdisciplinary approach bridges soil, water, climate, and human systems, enabling him to address complex environmental challenges. He has contributed to national projects funded by major Taiwanese agencies and collaborated across borders on eight international research initiatives. He has led over NT$1.100 billion in academia-industry research, secured 7 major technology transfers valued at NT$12 million, and received a NT$500,000 licensing deal for a patented innovation. His technical achievements extend to 14 approved patents and over 100 SCI journal publications, cited more than 2.100 times in the past five years, with an h-index of 27. These accomplishments earned him Taiwan's National Innovation Award in Environmental Technology and Energy Applications. Dr. Wen is also a dedicated educator, having mentored dozens of master's and doctoral students while delivering high-level instruction in fluid mechanics, hydrogeology, disaster prevention, and basin management. He serves as Director of the Micro- Hydropower Research Center and the Research Center for Soil & Water Resources and Natural Disaster Prevention, reinforcing collaboration among academia, government, and industry. His leadership has guided the implementation of social responsibility initiatives recognized with the TSAA Taiwan Sustainability Action Award in 2023 for SDG6. A recipient of prestigious honors from the Ministry of Economic Affairs, the Water Resources Agency, and civil engineering societies, Dr. Wen exemplifies academic and professional excellence. He has played vital roles in the Chinese Institute of Engineers, served on the Ministry of Education's safety advisory committee, and continues to influence environmental and disaster management policy and education in Asia. His career illustrates how rigorous research, practical implementation, and public service can converge to create lasting societal value.

Dr. Kun-Yi Andrew Lin received his Ph.D. from the Department of Earth and Environmental Engineering at Columbia University (USA). He is currently working as a Professor in the Department of Environmental Engineering. His research focuses on development of advanced materials and catalysts for energy and environmental applications. In the past few years, he has been becoming one of leading experts for environmental applications of metal organic frameworks (MOFs) and their derivatives. From February 2024, Prof. Lin will join the Institute of Analytic and Environmental Sciences at National Tsing Hua University (Hsinchu City, Taiwan) as a joint-appointment professor.

Dr. Yuvaraja Gutha obtained his M.Sc. degree in Physical Chemistry from Sri Venkateswara University, Tirupati, India, in 2009. He pursued his Ph.D. at the same institution and received his degree in 2014. During his doctoral studies, he worked as a Senior Research Fellow under the University Grants Commission (UGC), New Delhi, India. In 2016, Dr. Gutha Yuvaraja moved to Tianjin University, China, for postdoctoral research, focusing on the removal of heavy metals and dyes from wastewater. Dr. Gutha Yuvaraja published more than 35 research articles in reputed international journals. From 2018 to 2020, he continued postdoctoral work at Guangzhou University, China, under the supervision of Prof. Diyun Chen and Prof. Lingjun Kong, and focuses on U(VI) removal using various natural and chitosan-modified materials as adsorbents. Currently, he is working as a postdoctoral fellow at National Yunlin University of Science and Technology, Taiwan, where he continues his research in environmental remediation and waste water treatment.

Prof. Chi-Min Shu is a Distinguished Chair Professor in Department of Safety, Health and Environmental Engineering at National Yunlin University of Science and Technology, Taiwan. Prof. Shu is a chemical engineering graduate and migrated towards the process safety upon the thrust towards the industrial safety. Prof. Shu, initiated a prodigious impulse in the field of process safety research by establishing the Process Safety and Disaster Prevention Laboratory (PS&DPL), Taiwan. The focus of PS&DPL is primarily on loss prevention, thermo-kinetic hazard analysis, runaway reaction analysis, combustible gas or dust explosion analysis, risk assessment, and process-safety-related problems. In the past decade, I have received the North American Thermal Analysis Society (NATAS) Fellow Award in 2011 and in 2016 was elected as an American Institute of Chemical Engineers Fellow. In 2017, our continuous contribution was recognized by receiving the NATAS Mettler Toledo Award, the most honorable award in the field of Thermal Analysis since 1968. Prof. Shu expertise in process safety led him the invitation from various Governments across the globe to be a part of investigation teams. For instance, the most famous the underground pipeline explosion that occurred in August 2014 in Kaohsiung, Taiwan, which is a well-known disaster is one among them. Since 2005, Prof. Shu have been a Advisory Board Member of Fire Accident Investigation in (1) the National Fire Agency, Ministry of the Interior, (2) Taichung City, and (3) the Yunlin County Fire-Fighting Department. In 2015, I was the first scholar in the field of chemical process safety to assume an office at the Environmental Impact Assessment (EIA) Committee, accredited by Environmental Protection Administration of the Executive Yuan, Taiwan. To date, Prof. Shu reviewed more than 500 EIA reports and attended more than 100 EIA meetings. Prof. Shu is continuously striving to overcome challenges to industrial safety by intensively publishing papers in various respected international scientific journals. His laboratory findings have been documented through publications (350+) in reputed science journals of loss prevention and process safety. About academic dedication, Prof. Shu is serving as an editorial board member in various respected scientific journals, such as Process Safety Progress (SCI), Journal of Safety Research (SSCI), and Journal of Loss Prevention in the Process Industries (SCI) and as an associate editor for the Journal of Thermal Analysis and Calorimetry (SCI) during the periods 2009–2010 and 2018–2020.

Dr. Vijaya Yarramuthi received M.Sc. (2003), M.Phil. (2006) and Ph.D. (2009) in Chemistry from Sri Venkateswara University, Tirupati, Andhra Pradesh, India. Visiting Researcher at Research Centre for Soil & Water Resources and Natural Disaster Prevention, National Yunlin University of Science & Technology, Taiwan (2019). Dr. Vijaya presently working as Associate Professor in the Department of Chemistry, Vikrama Simhapuri University, Nellore, Andhra Pradesh, India. Her research interests are Adsorption Process in Water Treatment (Removal of metals, phenols, dyes and fluorides) and Design and synthesis of natural and synthetic adsorbents for water treatment.